Bull. Disas. Prev. Res. Inst., Kyoto Univ., Vol. 22, Part 3, No. 207, March, 1973 197

Earthquake Generating Stress in Eastern Chugoku and Northern Kinki Districts, Southwest Japan

by Ryōhei NISHIDA

(Received March 29, 1973)

Abstract

In order to clarify earthquake generating stress in the eastern Chugoku and the northern Kinki Districts and also to examine its relations to geological structures, 65 local earthquakes of magnitude $\geqq 2{\cdot}5$ in these districts for 5 years from 1966 to 1970 were analyzed.

By the use of the method of smoothed radiation pattern, the mean orientation of the maximum pressure axis of tectonic stress prevailing in the whole region was estimated to be nearly horizontal and E-W.

Next, the whole region was divided into 12 small regions, and two methods, the fault plane solution and the smoothed radiation pattern, were applied to earthquakes in respective regions. Fault plane solutions showed some features characteristic of the regions, which are interpreted to have some relations to geological structures. Also, the regional difference in directions of the maximum pressure axis was observed from smoothed radiation patterns in respective regions.

These facts probably point out that earthquakes in this area are generated under a common tectonic stress of E-W compression and that geological structures act to give a preferred orientation of fracture.

1. Introduction

It is well known that recent studies of focal mecanism of large earthquakes, which have occurred in island arcs or continental margins have greatly contributed to the development of global tectonics. On the other hand, microearthquakes occurring inland have been investigated by many seismologists, giving various knowledges of seismicity and related statistical properties. These studies of microearthquakes seem to point out that microearthquakes will be very useful for clarifying relations between earthquake occurrence and tectonics.

As for the northern Kinki and the eastern Chugoku Districts, some researches have been published. Hashizume discussed that on the basis of hypocenteral distribution of microearthquakes in this district from 1964 to 1968 the occurrence of microearthquakes is related to the nature of the upper crust, and that most of microearthquakes occur down to a depth of 15 km. Although his analysis of focal mechanism seem somewhat insufficient, he concluded that the mean direction of the maximum pressure axis in this district is E–W.[1)2)3)] Ichikawa investigated in detail the focal mechanism of earthquakes of magnitude more than 4.0 in this district.[4)] Aki concluded that earthquake generathing stresses of a series of earthquakes in 1960, in southern Hyogo Pref., lie nearly horizontally in E–W direction, using a method of smoothed radiation pattern.[5)] Nakamura analized the focal mechanism of local earthquakes in the northern Kinki District, and showed that the maximum pressure axis lies also

nearly in E-W direction.[6]

From view point of geology, Huzita argued that occurrence of microearthquakes is related to active faults, e.g. the Yamasaki Fault and the Mitoke Fault, and explained this phenomenon by assuming that seismically active zones correspond to shear zones in the crust.[7]

In the Outer Zone of Kinki, on the other hand, Shiono investigated local and microearthquakes in the Kii Peninsula, discussing the relations between earthquake mechanisms and tectonics.[8][9][10]

Under these circumstances, it seems important to investigate in more detail properties of local and microearthquakes. Since in the Kinki and Chugoku Districts the networks of Microearthquake Observatories are densely distributed, these districts offer very favorable conditions for the above purposes.

In the following, we shall discuss fault plane solutions and smoothed radiation patterns of local earthquakes and try to infer earthquake generating stress in the northern Kinki and the eastern Chugoku Districts.

2. Data and Methods used

We analyzed 65 earthquakes of magnitude more than 2.5 occurring in this district for 5 years from the beginning of 1966 to the end of 1970. In this district about 400 microearthquakes have occurred for one year and their hypocenters have been determined regularly by the Tottori Microearthquake Observatory. Throughout this study hypocenters were determined by the same method as above.[11]

Their magnitudes are those determined by J.M.A.. However, as for the earthquakes whose magnitudes were not determined by J.M.A., the following method was used.[12] Fig.1 shows a relation between the magnitude determined by J.M.A. and

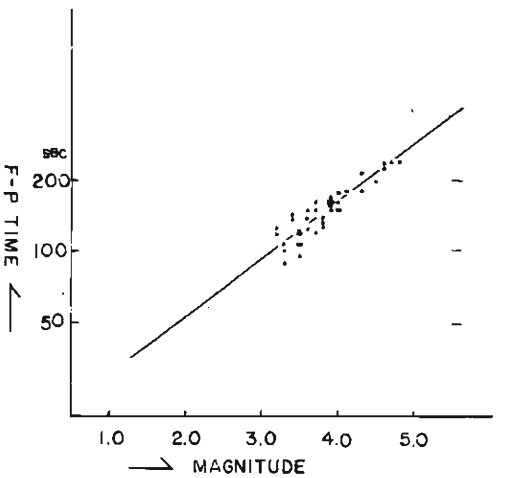

Fig.1 The relation between F-P time observed by five stations (belonging to the Tottori Microearthquake Observatory) and Magnitude determined by J.M.A..

F-P time of each earthquake which is the time duration from the onset of the initial P motion to the coda. An empirical equation is derived from this figure as follows:

$$M = 4.1 * \log (\text{F-P time}) - 5.1,$$

and unknown magnitudes are determined from this equation by use of their F-P times. Table 1 lists the origin time, epicenter, focal depth and magnitude of these

Table 1 List of earthquakes. Np, N+ and N− show numbers of initial P motion, compression and dilatation, respectively. Azimuth (φ) is measured clockwise from the north, θ is measured downward from the vertical.

No.	Origin Time					MAG	Epicenter		De-pth	P-Data			P-axis		T-axis		Region
	Y	M	D	H	M		Latitude	Longitude		Np	N+	N−	Azi-muth	θ	Azi-muth	θ	
							° ′ ″	° ′ ″	km				°	°	°	°	
1	66	3	10	12	48	4.6	35 9 53	135 48 15	27	22	10	12	85	75	265	16	
2			11	21	55	3.2	35 4 3	135 42 16	10	11	2	9					9
3			12	1	27	3.7	34 55 43	133 22 13	10	11	4	7					2
4			18	9	24	3.3	35 1 34	135 35 34	13	13	7	6	72	90	162	90	9
5			18	12	18	3.6	35 0 58	135 36 25	12	12	7	5	73	90	163	90	9
6			30	17	3	3.0	35 1 34	135 39 15	12	14	8	6					9
7		4	16	20	43	3.4	34 39 33	135 3 53	12	21	13	8	238	54	19	42	5
8			17	3	41	3.5	34 41 43	135 2 17	15	21	11	10	95	65	2	86	5
9		6	15	17	30	4.5	34 57 7	135 23 28	5	30	12	18	291	86	24	66	9A
10			29	21	22	4.7	34 49 49	135 25 7	13	34	17	17	276	69	14	69	6A
11		7	26	21	6	3.7	34 36 47	135 17 25	12	18	8	10	317	85	224	56	6B
12			28	4	17	2.9	34 36 54	135 17 21	15	16	9	7	119	83	210	83	6B
13		10	3	5	31	3.8	34 54 32	135 35 2	13	19	9	10					9A
14		11	4	5	39	3.6	34 57 11	135 41 56	9	18	13	5	86	55	176	85	9
15			12	22	25	4.0	35 19 41	135 41 40	8	16	6	10	226	62	355	42	8
16		12	10	19	38	3.6	35 23 11	134 15 58	3	13	4	9	263	53	180	82	1
17			31	13	4	2.5	34 46 54	135 56 8	3	15	2	13					
18	67	1	2	5	36	3.9	34 42 48	133 28 0	19	14	5	9					2
19			14	11	48	2.8	34 57 4	135 41 1	5	19	11	8	262	63	165	76	9
20		2	9	7	6	2.7	34 57 50	135 40 37	5	17	10	7	265	69	357	83	9
21		3	6	17	28	2.8	34 26 37	133 56 55	19	7	3	4					2
22			10	19	32	2.7	34 43 30	135 15 27	11	20	11	9	289	83	20	83	6A
23			29	16	46	4.3	34 38 57	135 3 41	12	18	10	8	257	73	353	73	5
24		4	10	23	47	3.2	34 34 34	135 2 42	9	21	5	16	273	85	165	13	5
25			23	8	15	3.1	34 36 57	133 29 34	17	12	3	9					2
26			27	14	41	3.5	34 53 27	135 32 5	13	21	9	12	265	84	175	84	9A
27		6	21	21	9	4.6	34 59 30	135 33 4	5	27	13	14	276	72	175	57	9
28	67	7	1	19	5	3.8	34 55 4	135 28 47	19	24	7	17					9A
29			22	13	35	3.5	35 19 57	135 39 18	9	14	4	10	238	66	122	50	8
30		9	22	7	27	3.2	35 21 54	133 44 29	2	9	1	8					1
31		10	3	14	12	4.0	35 24 7	133 28 39	4	16	9	7	111	75	333	18	1
32		11	4	8	9	3.4	35 1 11	135 38 8	11	19	10	9	80	90	170	90	9
33			9	4	8	3.6	35 43 22	134 53 22	10	12	4	8					3

No.	Origin Time					MAG	Epicenter		Depth	P-Data			P-axis		T-axis		Region
	Y	M	D	H	M		Latitude	Longitude		Np	N+	N−	Azimuth	θ	Azimuth	θ	
							° ′ ″	° ′ ″	km				°	°	°	°	
34			28	22	52	3.0	34 46 35	135 21 50	12	17	9	8	284	80	16	80	6A
35		12	1	2	14	3.1	35 45 58	135 11 26	11	12	7	5					3
36	68	1	20	11	31	4.4	34 55 11	135 39 26	12	31	12	19	271	89	181	75	9
37			24	16	51	4.0	35 50 7	134 54 44	6	9	6	3					3
38		2	14	11	31	4.8	35 17 24	135 26 49	14	21	10	11	67	90	157	90	7
39		8	18	16	12	5.6	35 15 14	135 21 18	5	21	8	13	85	90	175	90	7
40			27	21	58	5.1	35 2 48	135 39 42	11	21	10	11	84	87	352	50	9
41			27	22	53	4.4	35 0 25	135 49 6	11	22	8	14	35	90	175	90	9
42		9	3	3	42	3.2	34 58 58	135 43 43	7	19	6	13	87	90	177	90	9
43			7	1	36	4.6	35 15 14	135 17 21	10	22	7	15	266	72	8	56	7
44			11	14	49	4.0	35 15 21	135 16 58	12	19	7	12	83	63	188	63	7
45			26	6	51	3.6	34 52 15	134 58 10	8	16	5	11	100	90	10	90	4
46		10	6	4	36	4.3	35 16 13	135 16 46	11	19	9	10	85	90	175	90	7
47		11	11	1	15	3.3	35 15 24	135 43 15	8	16	4	12	92	64	325	39	8
48		12	19	6	50	4.1	35 14 23	135 18 40	3	14	4	10					7
49	69	1	2	21	36	3.7	35 5 4	135 33 55	14	20	8	12	83	84	350	62	9
50		2	18	16	57	4.3	34 56 41	134 11 38	17	26	9	17	262	69	164	69	2
51		3	15	10	23	3.9	34 57 53	135 34 58	12	25	12	13	96	87	345	19	9
52		6	14	1	3	3.5	34 48 38	134 45 1	10	19	8	11	282	75	188	75	4
53			16	18	53	3.3	34 49 56	134 44 45	15	18	9	9	280	67	21	67	4
54			17	1	45	3.9	35 24 33	134 0 28	9	15	9	6					1
55	69	6	20	15	33	3.5	34 55 59	135 5 4	13	13	5	8					4
56			20	16	7	3.5	34 55 46	135 5 39	14	19	5	14	263	77	8	38	4
57		10	12	4	54	3.8	35 14 23	135 10 23	12	17	9	8	90	90	180	76	2
58		12	20	21	16	3.9	34 39 56	133 36 40	10	12	6	6	286	76	20	76	2
59	70	1	3	14	42	3.7	35 36 26	135 18 40	33	15	14	1					
60		3	23	6	55	3.8	35 16 19	135 52 11	8	16	6	10					8
61		4	3	10	2	3.8	35 3 11	134 54 53	11	24	11	13					4
62			7	1	41	4.3	35 17 47	134 14 16	5	34	11	23	98	76	192	76	1
63		8	5	22	59	3.9	34 44 49	134 16 46	5	24	11	13					2
64			21	3	47	3.5	34 46 5	135 34 35	13	19	7	12	283	77	17	77	9A
65		11	30	13	15	3.7	34 41 56	134 52 27	14	23	11	12					4

earthquakes. Distributions of epicenter and focal depth are shown in Fig. 2 and Fig. 3, respectively. The majority of earthquakes in this district are distributed in the upper crust down to 20 km of depth and it is noticed that this distribution of focal depth is the same as that obtained by microearthquakes.[13]

The distribution of observations at which the initial P motions were read is shown in Fig. 4, which are attached to the Japan Meteorological Agency, Wakayama Microearthquake Observatory, Shiraki Microearthquake Observatory, Kochi Seismological Observatory, Abuyama Seismological Observatory and the Tottori Microearthquake Observatory. In Table 1 the numbers of initial P motion used for the analysis are listed. The initial P motions were observed at about 18 stations for respective

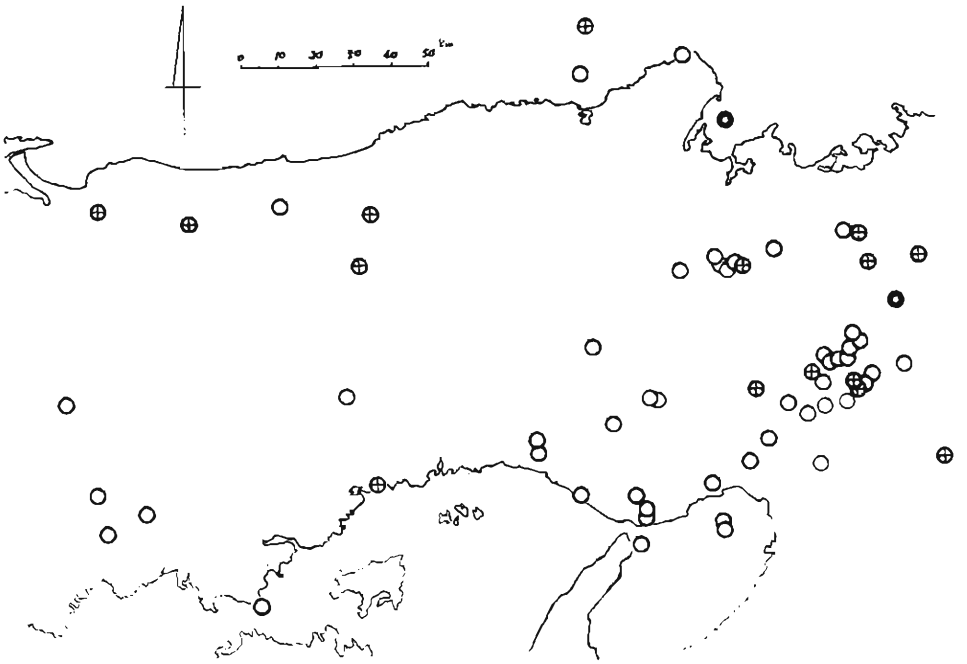

Fig. 2 The epicenter distribution of local earthquakes of $M \geq 2.5$ for five years from 1966 to 1970.
⊕ : Focal depth is 0 km to 8 km.
○ : Focal depth is 9 km to 20 km.
◎ : Focal depth is more than 21 km.

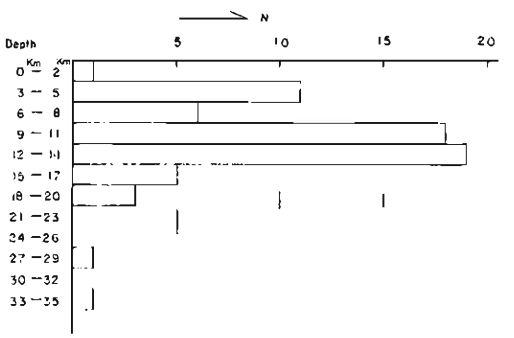

Fig. 3 Distribution of focal depth. Abscissa and ordinate show frequency of earthquakes and focal depth in km, respectively.

earthquakes. Distributions of directions of the initial P motions on upper hemisphere by the Wulff's net projection are shown in Fig. 7 to Fig. 20. Fault plane solutions could be determined for 44 earthquakes, in which there were eight dip slip fault types. The directions of the maximum pressure axis (P-axis) and the minimum

Fig. 4 The location of observation stations.

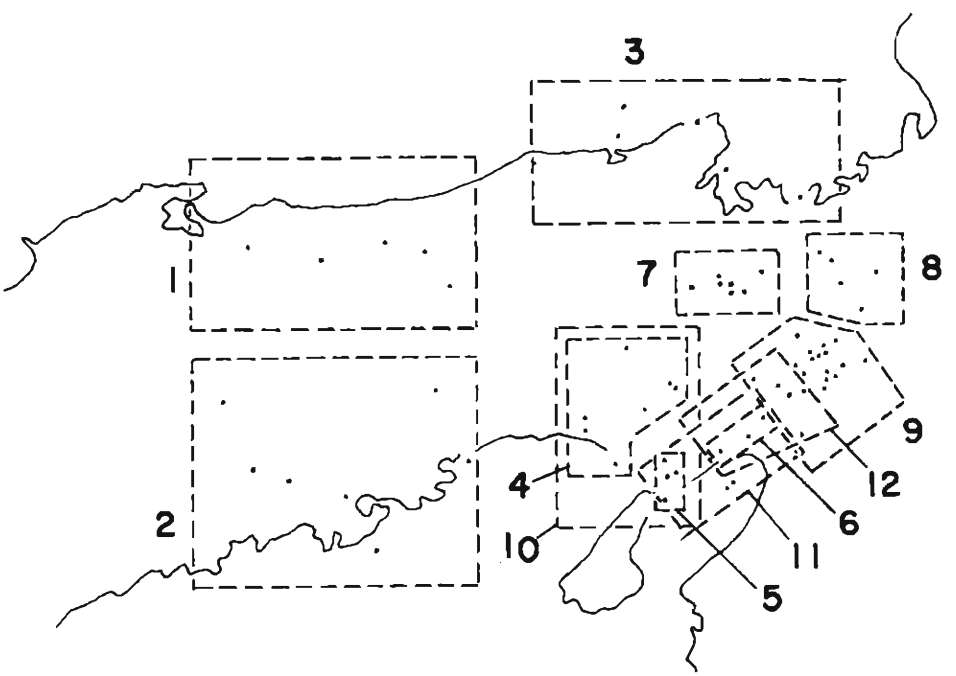

Fig. 5 Division of the area concerned.

pressure axis (T-axis) are shown in Table 1.

If earthquakes were generated by the same tectonic stress acting in a wide area, the maximum pressure axis of individual earthquake is expected to have nearly the same direction. Hence it is necessary to determine the mean orientations of the principal stresses in each small region. On this account, the whole region was divided into 12 regions as shown in Fig.5. Numbers of earthquakes and the initial P motions used in the present analysis are listed in Table 2.

Table 2 List of number of earthquakes and initial P motion in each region.

Region	Number of Earthquakes	Np	N+	N−
1	5 (3)	87	34	53
2	7 (2)	106	41	65
3	3	33	17	16
4	7 (4)	132	54	78
5	4 (4)	81	39	42
6	3 (3)	71	37	34
7	7 (6)	133	54	79
8	4 (3)	62	20	42
9	20 (16)	400	181	219
10	11 (8)	213	93	120
11	9 (9)	186	93	13
12	8 (6)	184	81	103
Total	62 (41)	1139	494	645

In this study the method of smoothed radiation pattern which was used by Aki (1966) and Oike (1971) is adopted.[14][15] The method is to determine the mean solution for each group of earthquakes by superposing all initial P motions as if they came from the same single source. The distribution of the initial P motions superposed on a upper focal hemishere is smoothed and normalized by the following procedure. Numbers, N− (compressions) and N+ (dilatations) within an angular distance of 45° from Q (θ, φ) and its antipode Q′ $(\pi-\theta, \pi+\varphi)$ on the focal sphere, are counted. Then a normalized parameter K (θ, φ) was calculated by the following formula,

$$K = \frac{N+ - N-}{N+ + N-} .$$

The parameter K (θ, φ) was calculated for 70 points of Q (θ, φ) as follows ;

$\theta = 10°$, $\varphi = 0°, 90°, 180°, 270°$

$\theta = 30°$, $\varphi = 0°, 30°, 60°, 90°, 120°, 150°, 180°, 210°, 240°, 270°, 300°, 330°$

$\theta = 50°$, $\varphi = 0°, 20°, 40°, 60°, 80°, 100°, 120°, 140°, 160°, 180°, 200°, 220°, 240°, 260°, 280°, 300°, 320°, 340°$

$\theta = 70°$, $\varphi = 0°, 20°, 40°, 60°, 80°, 100°, 120°, 140°, 160°, 180°, 200°, 220°, 240°, 260°, 280°, 300°, 320°, 340°$

$\theta = 90°$, $\varphi = 0°, 10°, 20°, 30°, 40°, 50°, 60°, 70°, 80°, 90°, 100°, 110°, 120°, 130°, 140°, 150°, 160°, 170°$

where θ is measured downward from the vertical and φ is measured clockwise from

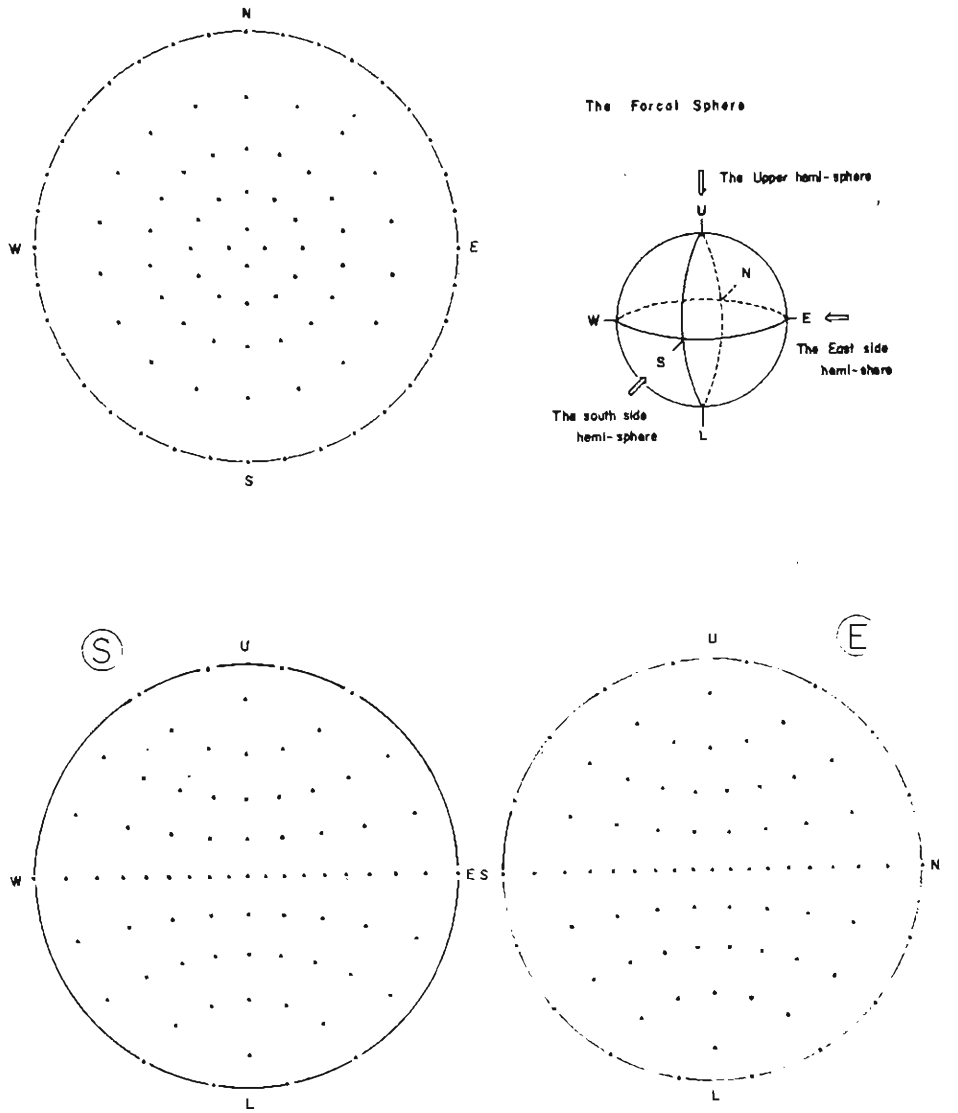

Fig. 6 Explanation of the smoothed radiation pattern and the distribution of point Q (θ, φ) on the upper, east-side and south-side hemisphere using Wulff's net.

the north. Distribution of points Q (θ, φ) is shown in Fig.6, which is composed of a set of figures projected on the upper, east-side and south-side hemisphere. The K-value is plotted at the corresponding point Q, and smooth lines are drawn connecting equal K-values. The maximum value of K on a focal sphere corresponds to the axis of the maximum pressure and the minimum value of K to the axis of the minimum pressure. Smoothed lines of equal K-value are shown in Fig.7 to Fig.

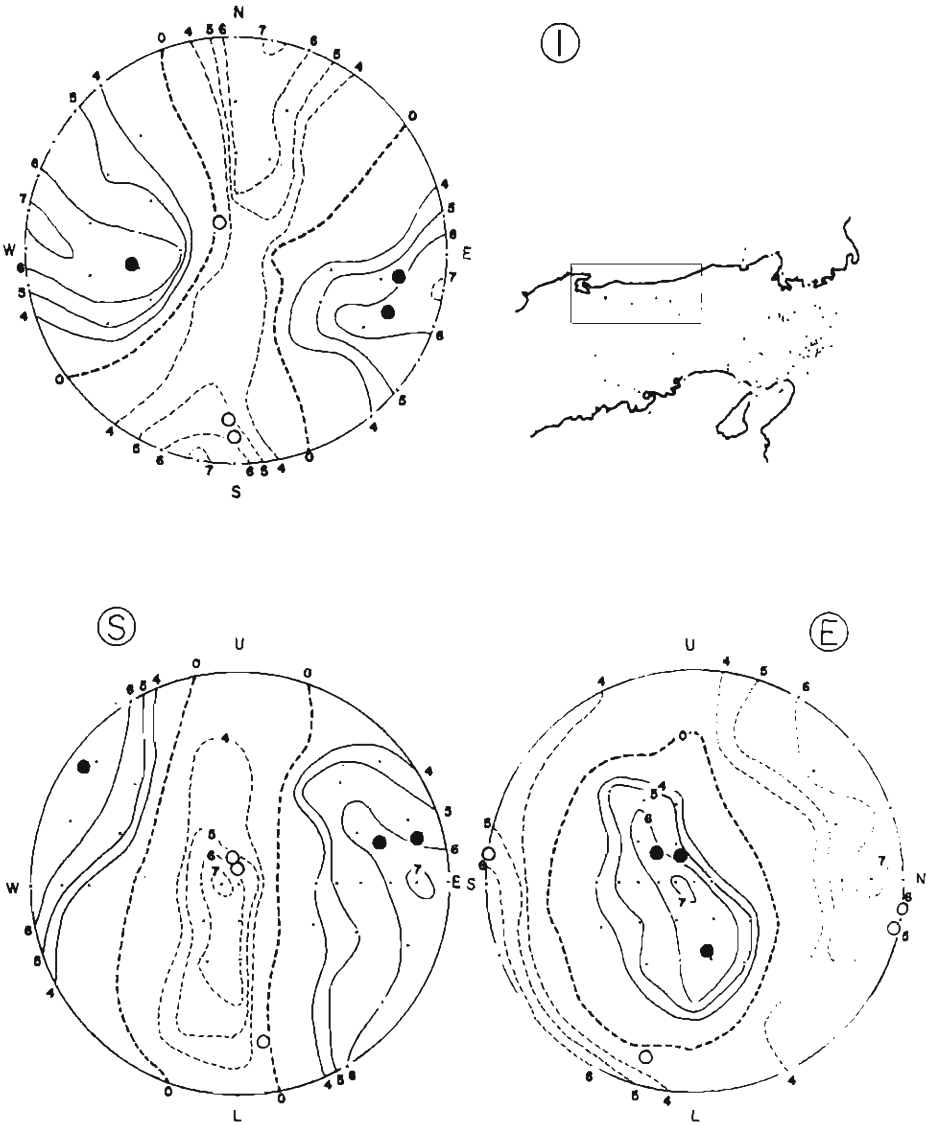

Fig. 7 (a) Smoothed radiation pattern of Region 1. Solid lines indicate equal lines of positive K-value and dotted lines indicate equal lines of negative K-value. Open and closed circles express P axis and T axis of fault plane solutions of respective earthquakes. Small closed circles indicate the points where magnitude of K-value is significantly great.

19. Throughout these figures, solid lines are used for positive K-value, dotted lines for negative K-value, and small closed circles indicate the points where the magnitude of K-value is significantly great.[16]

3. Results obtained for each region.

(*a*) *Region 1, Tottori Pref.* (No. 16, 30, 31, 54, 62)

Fig. 7(a)presents the smoothed radiation patterns on three hemispheres, and Fig.7(b) shows the fault plane solutions of respective earthquakes. The maximum pressure axis (P axis) turns clockwise by about 10° from the E-W direction, and likewise

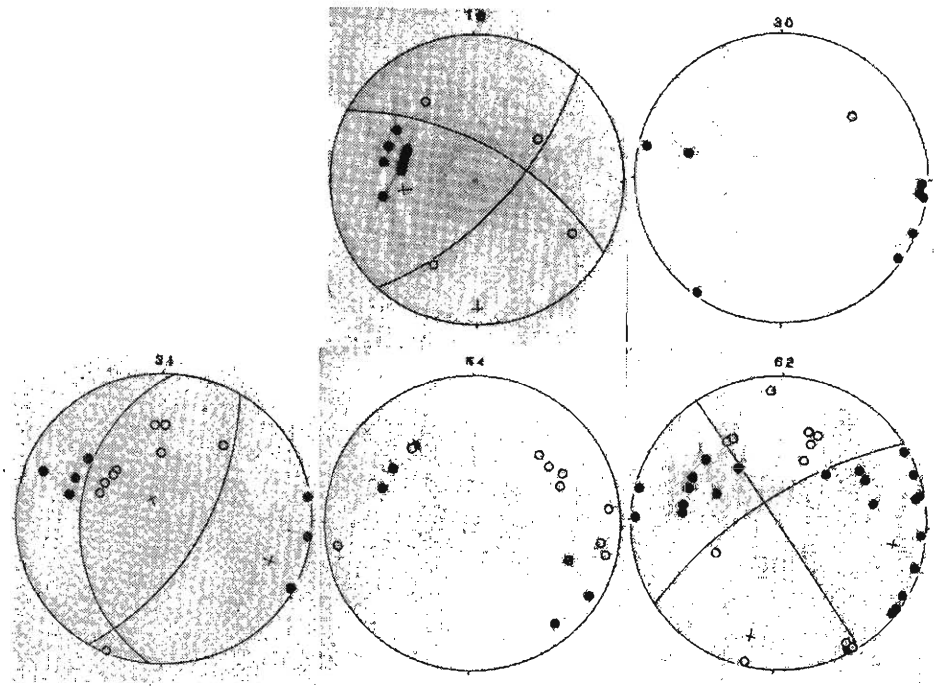

Fig. 7 (b) Individual fault plane solution and distribution of initial P motions projected by Wulff's net of upper hemi-sphere. Open and closed circles indicate compressions and dilatations, respectively. (Region 1)

the minimum pressure axis (T axis) turns clockwise by about 10° from the N-S direction. Contours of equal negative K-value are slender compared with those of positive value. An earthquake in the western Tottori Pref. (No. 31) has a focal mechanism of dip slip fault type whose axis of the maximum pressure lies in E-W. Focal mechanisms of earthquakes generated in the eastern Tottori Pref. are not necessarily the same as the focal mechanism of the Tottori Earthquake in 1943. The earthquake of No.62 seems to have some relation to the Yamasaki Fault inferred from its focal mechanism and position of epicenter.[17]

(*b*) *Region 2, Okayama Pref.* (No. 3, 18, 21, 25, 50, 58, 63)

As there are not sufficient numbers of observation stations in this region, only two earthquakes out of seven was it possible to obtain fault plane solutions (Fig. 8b). From the analysis of smoothed radiation pattern the maximum pressure axis lies in E-W direction dipping westward. Contours of equal positive K-value are pretty concentrated, but those of negative value are rather scattered.

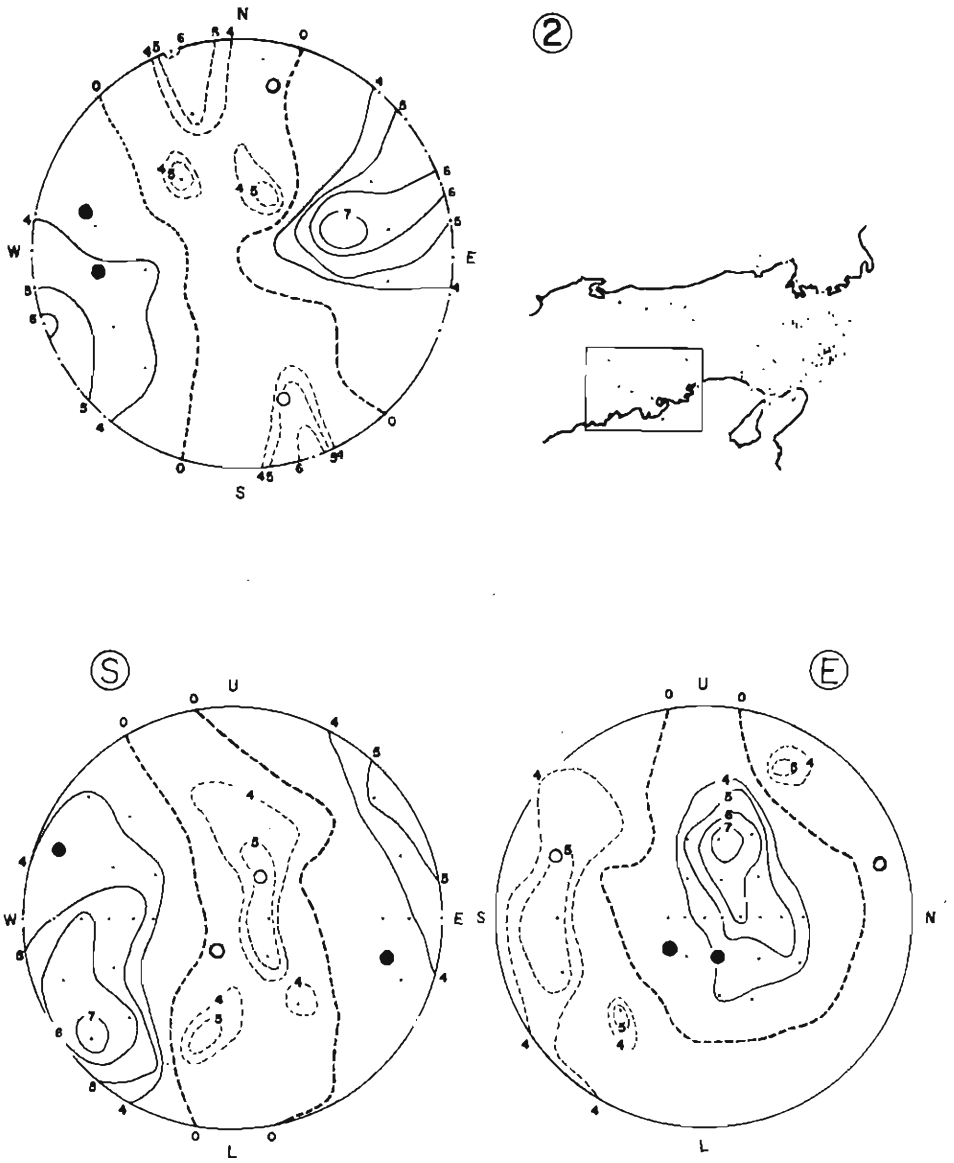

Fig. 8 (a) Smoothed radiation pattern of Region 2. The expression is the same as Fig. 7(a).

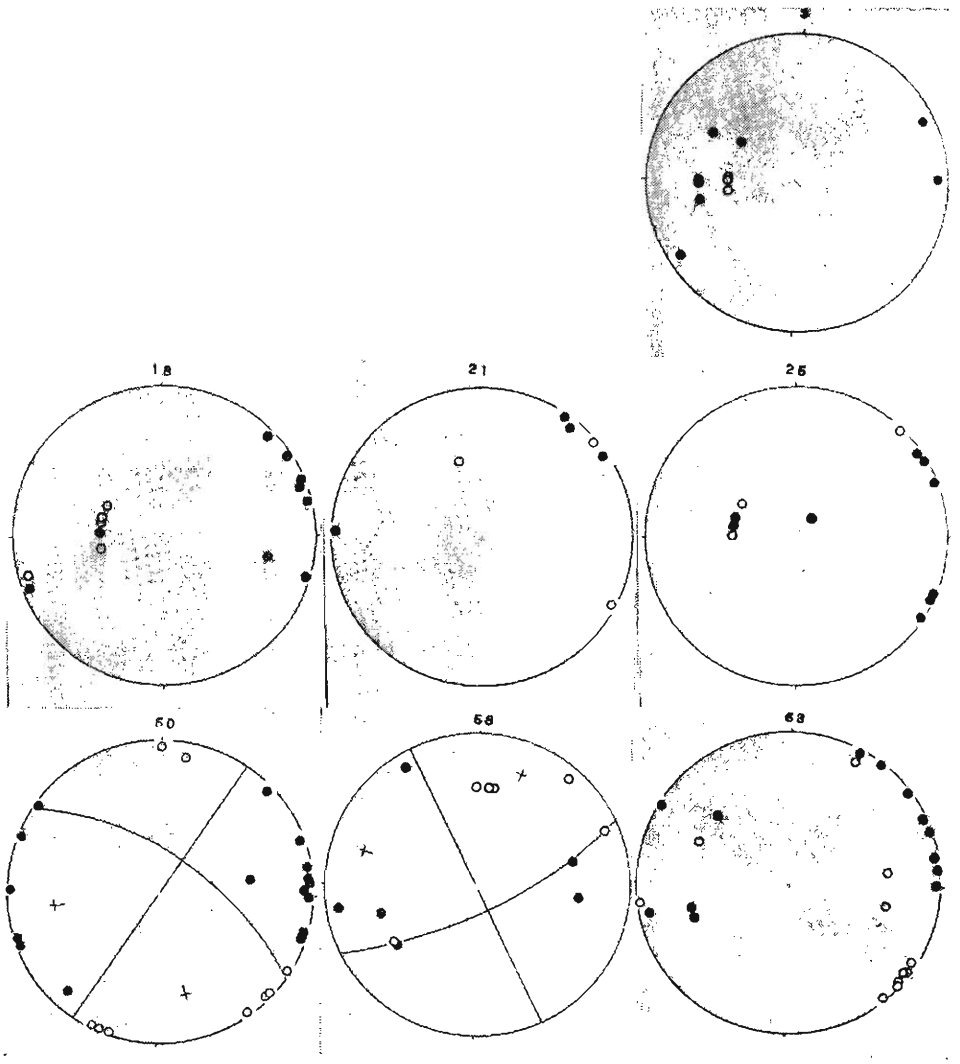

Fig. 8 (b) Individual fault plane solution and distribution of initial P motions projected by Wulff's net. The expression is the same as Fig. 7(b). (Region 2)

(*c*) *Region 3, Tango Region* (No. 33, 35, 37)

In this region the Tajima Earthquake (1925) and Tango Earthquake (1927) occurred and at present microearthquakes occur in and near the latter's aftershock area. However, the present analysis does not seem to give any conclusions, because of insufficient data. (Fig. 9)

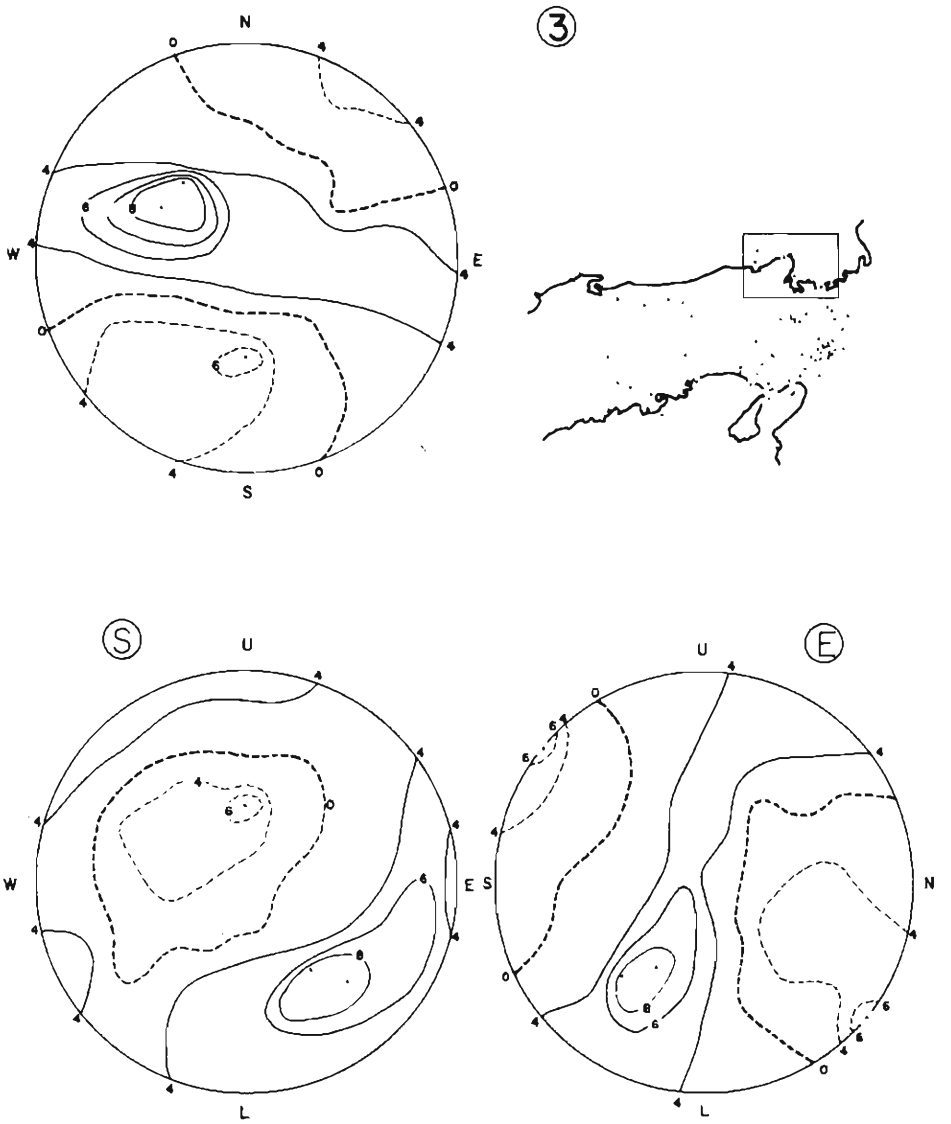

Fig. 9 (a) Smoothed radiation pattern of Region 3. The expression is the same as Fig. 7(a).

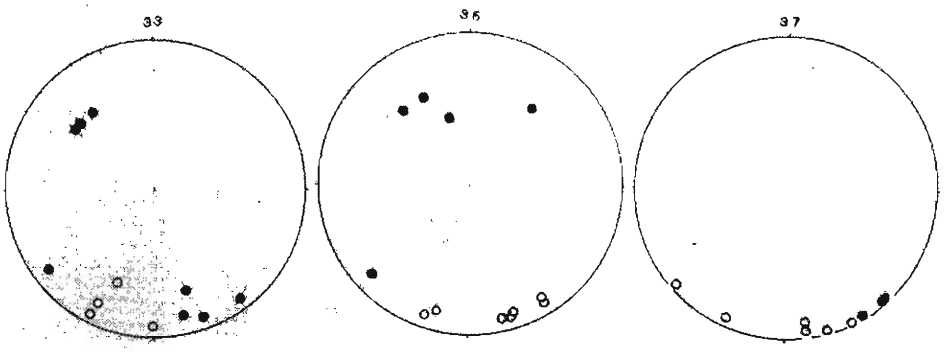

Fig. 9 (b) Individual fault plane solution and distribution of initial P motions projected by Wulff's net. The expression is the same as Fig. 7(b). (Region 3)

(*d*) *Region 4, Harima Region* (No. 45, 52, 53, 55, 56, 61, 65)

The smoothed radiation pattern and fault plane solutions in this region are shown in Fig. 10 (a) and (b), respectively. The high K-value zone corresponding to the maximum pressure is divided into two parts as shown in Fig. 10(a), but P-axes of respective earthquakes concentrate in an orientation dipped eastward by about 10° in E-W direction. The negative K-value zone corresponding to the minimum pressure lies in a direction with dip of about 50° southward. And directions of T-axes of respective earthquakes distribute in a slender zone of equal negative K-value. It is impossible to obtain focal mechanisms of No. 61 and 65 in spite of a sufficient number of observed data. It is to be noted that in this region and also in region 5 mentioned below T-axis is somewhat scattered in comparison with high concentration of P-axis.

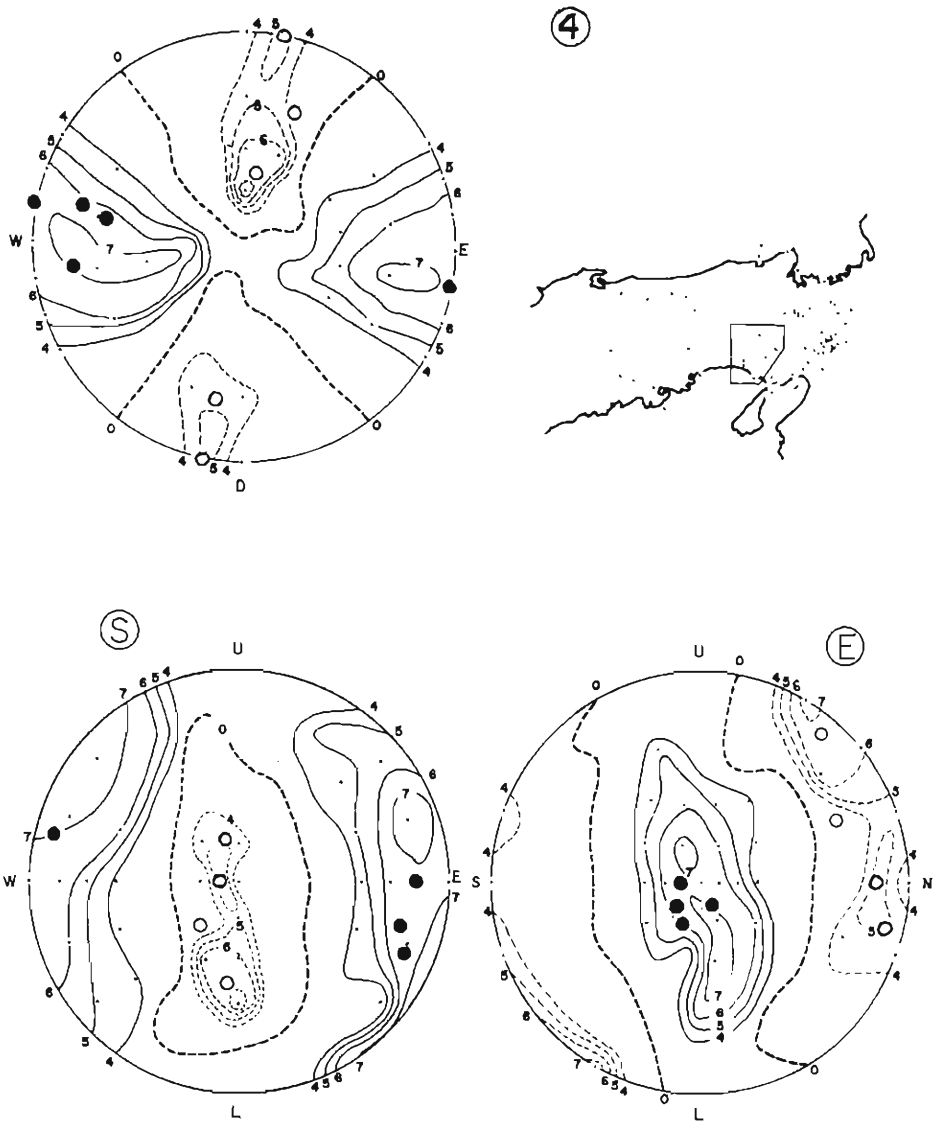

Fig. 10 (a) Smoothed radiation pattern of Region 4. The expression is the same as Fig. 7(a).

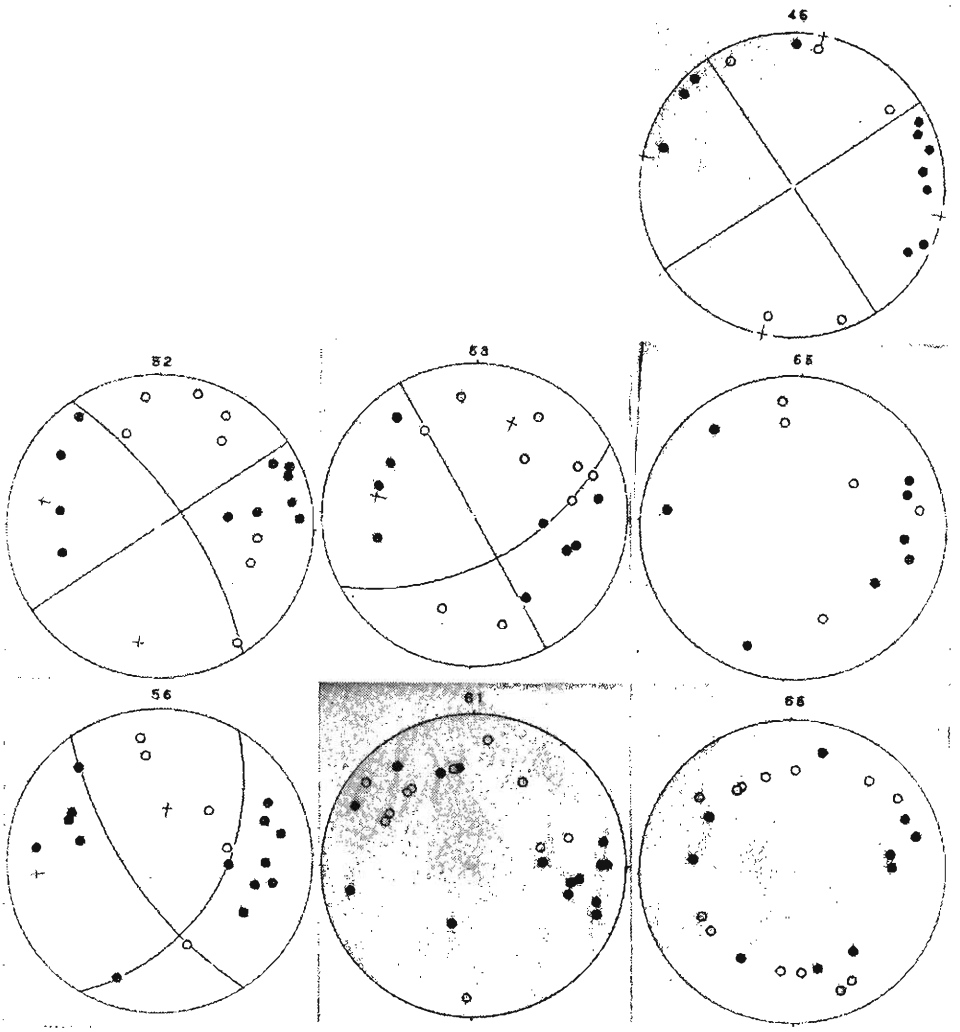

Fig. 10 (b) Individual fault plane solution and distribution of initial P motions projected by Wulff's net. The expression is the same as Fig.7(b) (Region 4)

(*e*) *Region* 5, *Akashi Straits* (No. 7, 8, 23, 24)

Fig. 11 shows the smoothed radiation pattern and fault plane solutions in this region. The maximum pressure axis lies in E–W direction dipped by about 20° eastward, and P-axes of fault plane solutions lie also in the same direction. But the zones of the minimum pressure concentrate in two parts in N–S direction. In particular, an earthquake at the southern part of Akashi Straits has a focal mechanism of clear dip slip fault type with E–W compression.

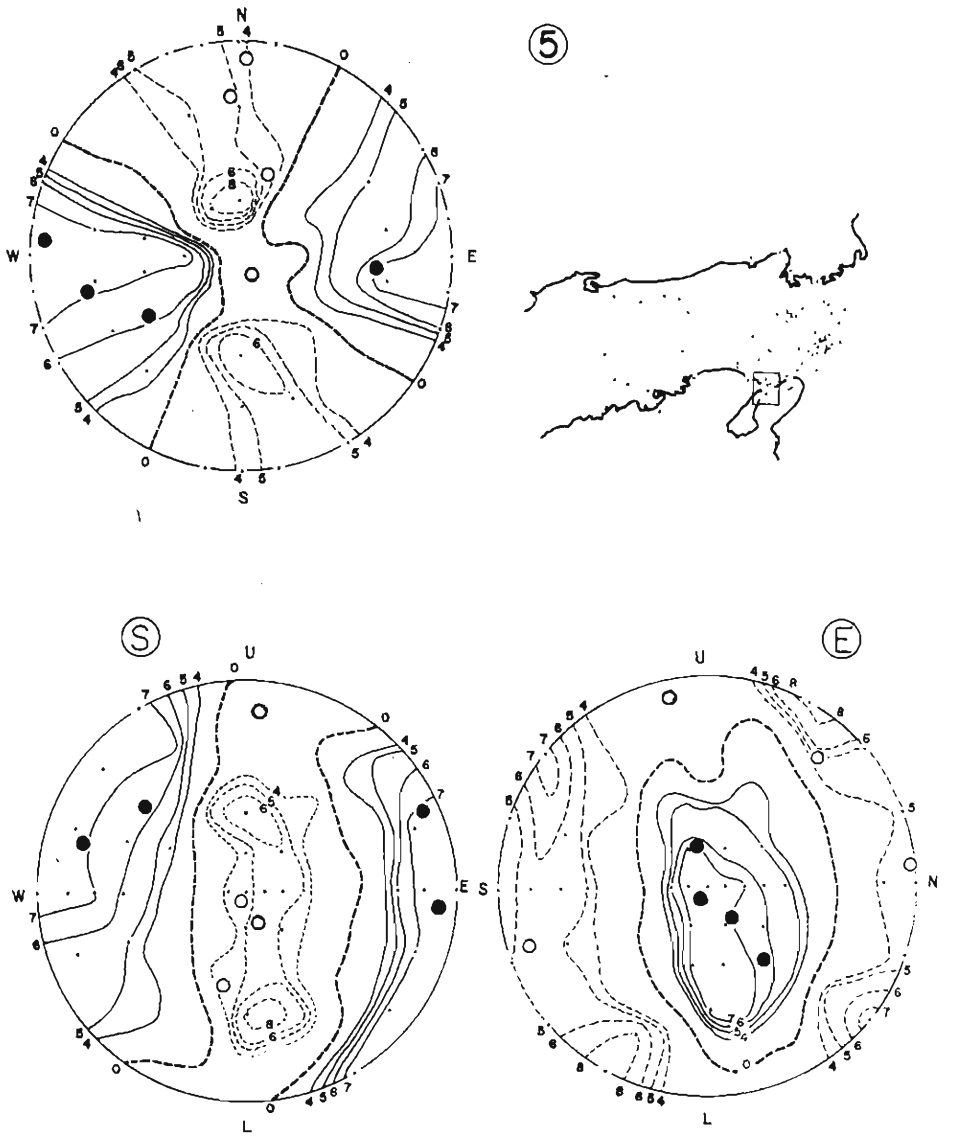

Fig. 11 (a) Smoothed radiation pattern of Region 5. The expression is the same as Fig. 7(a).

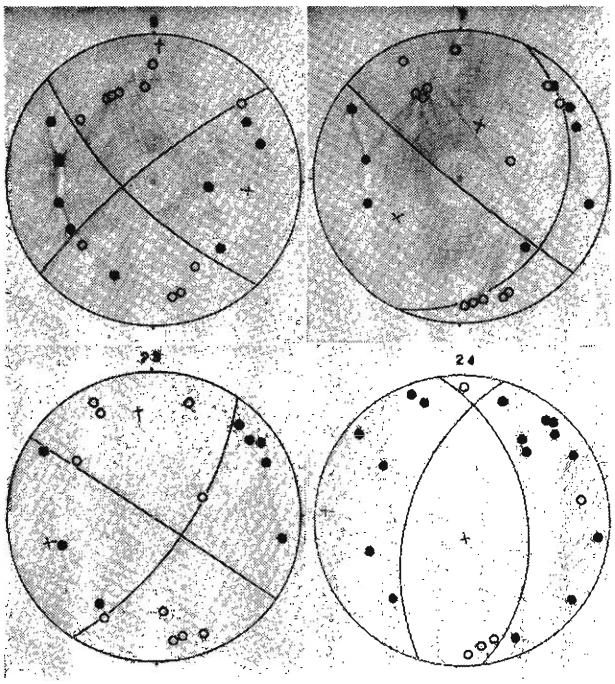

Fig. 11 (b) Individual fault plane solution and distribution of initial P motions projected by Wulff's net. The expression is the same as Fig.7(b). (Region 5)

(f) Region 6A, Rokko Region (No. 10, 22, 34)

Results of the smoothed radiation pattern and fault plane solutions in this region are shown in Fig.12(a) and(b). Three earthquakes had similar fault plane solutions and the same result was obtained from analysis of the smoothed radiation pattern. The maximum pressure axis is about 15° rotated clockwise from the E-W direction and dips about 10° eastward. The minimum pressure axis has a dip angle of 10° southward in the azimuth rotated 15° clockwise from N-S.

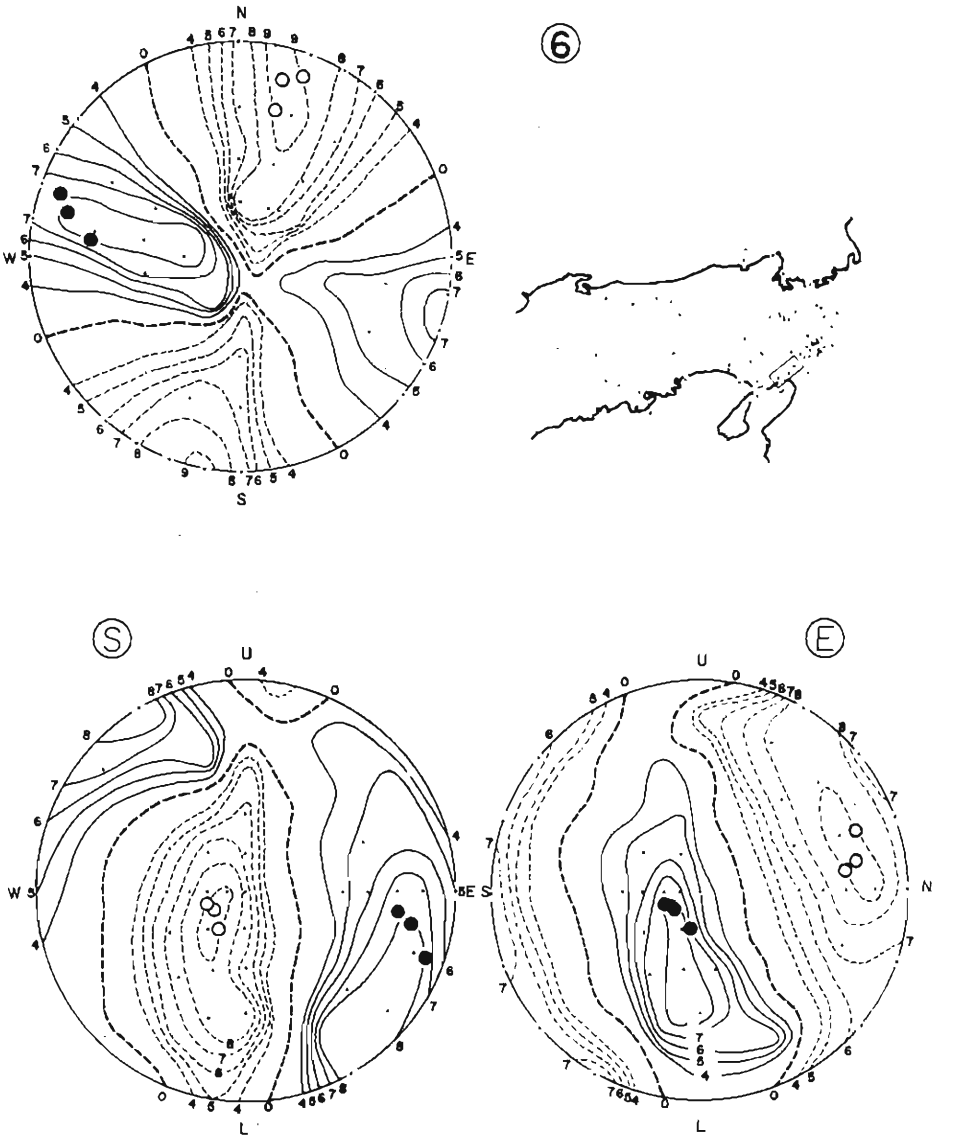

Fig. 12 (a) Smoothed radiation pattern of Region 6A. The expression is the same as Fig. 7(a).

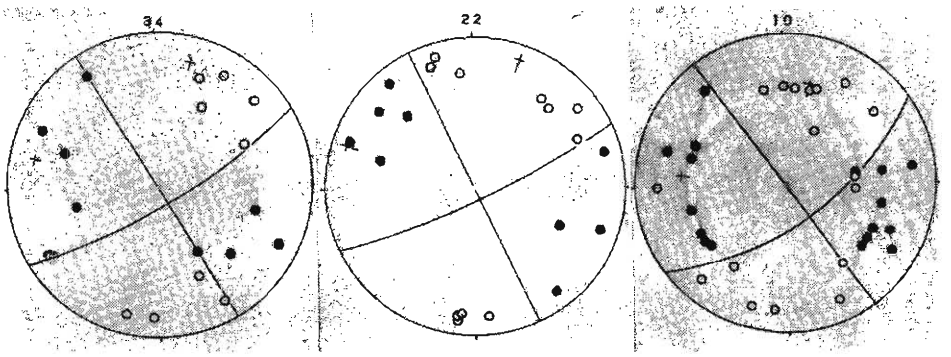

Fig. 12 (b) Individual fault plane solution and distribution of initial P motions projected by Wulff's net. The expression is the same as Fig. (7b). (Region 6A)

(g) *Region 6B, Osaka Bay* (No. 11, 12)

Fault plane solutions are shown in Fig. 13. The maximum pressure axes of two earthquakes rotate clockwise 47° and 29° from E–W direction, respectively. These deflection angles from E–W direction are the largest throughout the present analysis.

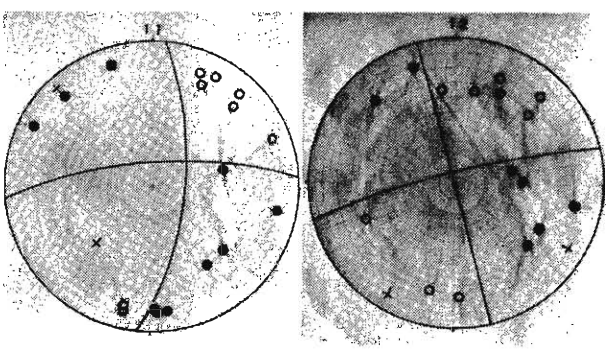

Fig. 13 Fault plane solution and distribution of initial P motions projected by Wulff's net. The expression is the same as Fig.7(b) (Region 6B)

(*h*) *Region 7, Wachi Region* (No. 38, 39, 43, 44, 46, 48, 57)

On August 18, 1968, an earthquake of magnitude=5.6 (No. 39) occurred at 135° 23' E and 35° 13' N. It was accompanied by many foreshocks and aftershocks, which continued for more than three years. A largest foreshock occurred on Feb. 14, 1968. Here seven earthquakes were analyzed, which consist of one foreshock, the mainshock and five aftershocks. The pattern in this region shows that the maximum

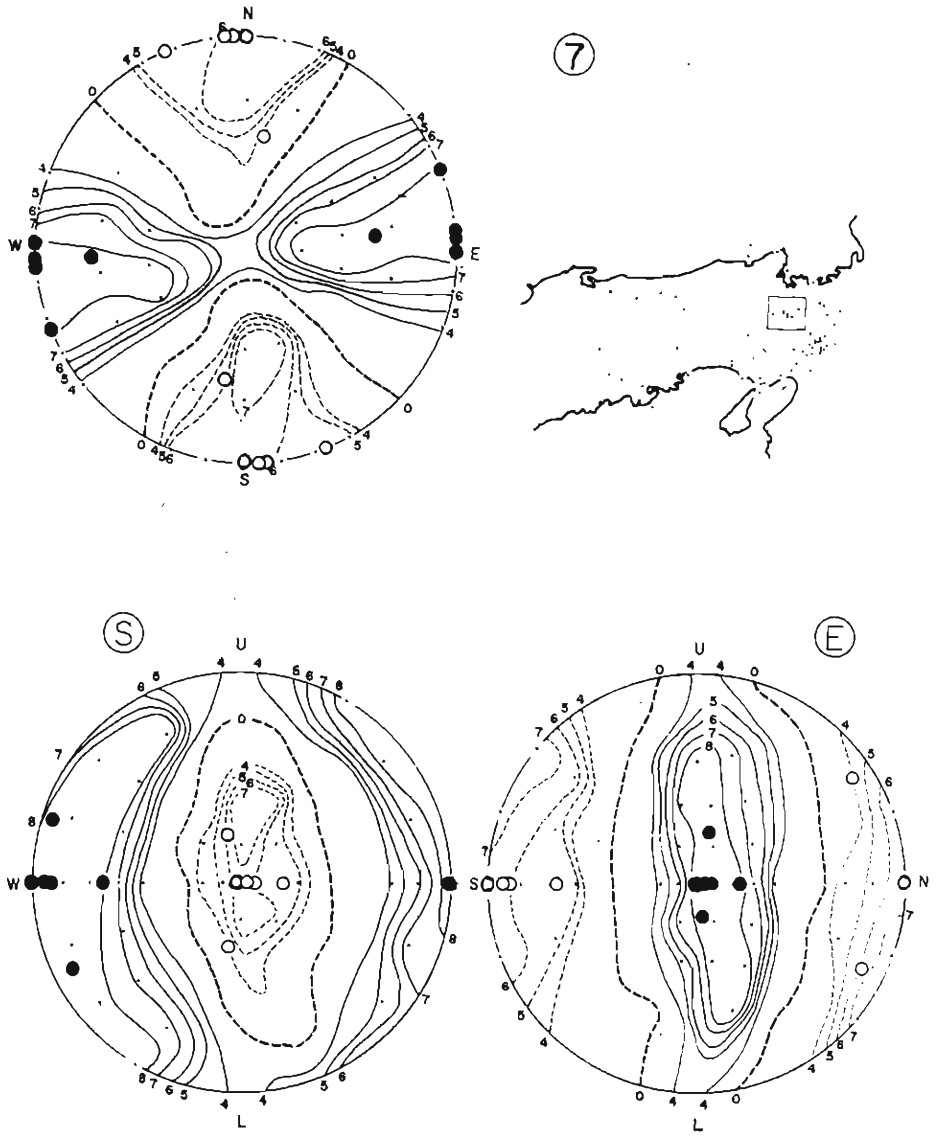

Fig. 14 (a) Smoothed radiation pattern of Region 7. The expression is the same as Fig. 7(a).

pressure axis lies nearly horizontally, and turns a little counterclockwise from the E-W direction. (Fig. 14(a)) Correspondingly, the minimum pressure axis lies nearly in the N-S direction. The focal mechanism of foreshock (No. 38) was different from the main shock and aftershocks, showing the maximum pressure axis rotated about 20° counterclockwise from the E-W direction. Focal mechanisms of aftershocks are similar to the mainshock.

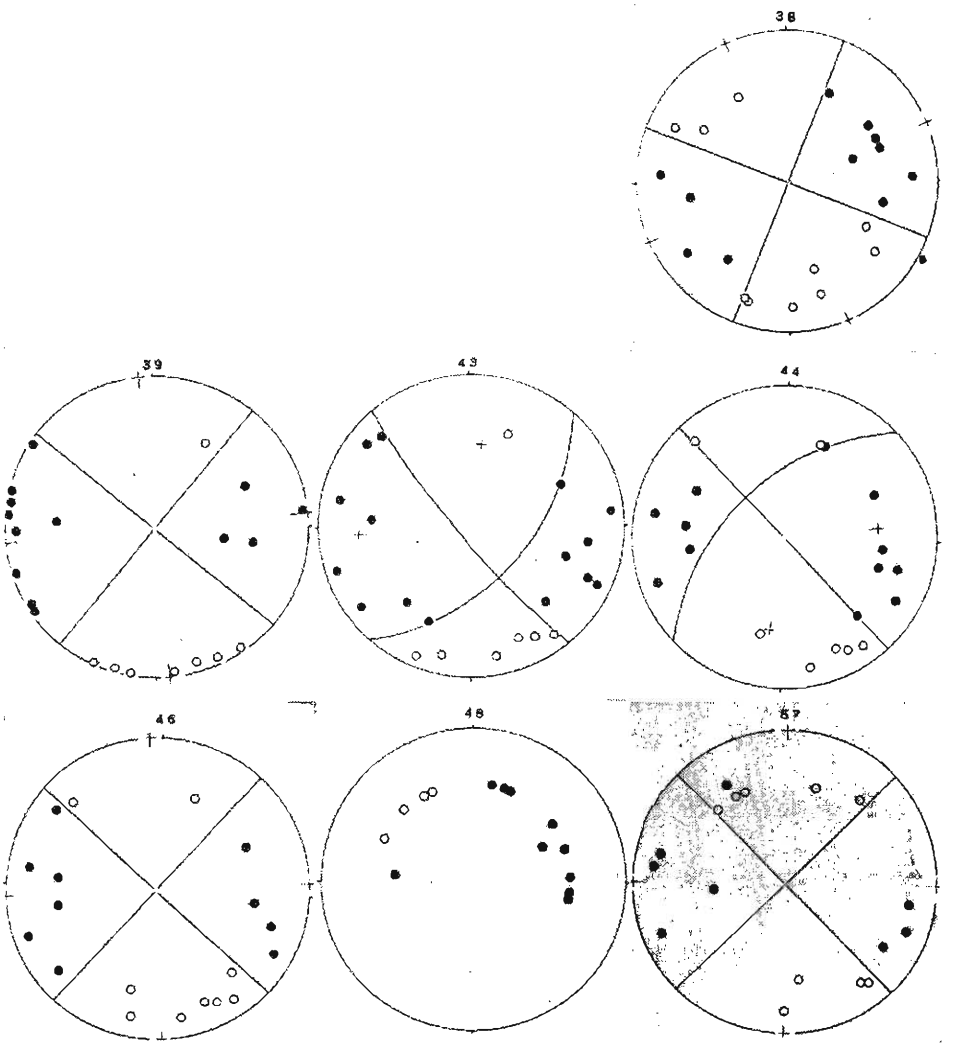

Fig. 14 (b) Individual fault plane solution and distribution of initial P motions projected by Wulff's net. The expression is the same as Fig. 7(b). (Region 7)

(i) Region 8, Northern Kyoto Pref. (No. 15, 29, 47, 60)

The smoothed radiation pattern and fault plane solutions in this region are shown in Fig.15(a) and(b). Fault plane solutions of all earthquakes show inclined null vectors. The pattern of this region shows that the orientation of the maximum pressure axis is deflected 15° from E–W direction, with a dip angle of 20° eastward. Although the contour of the positive K–value is concentrated and has larger values

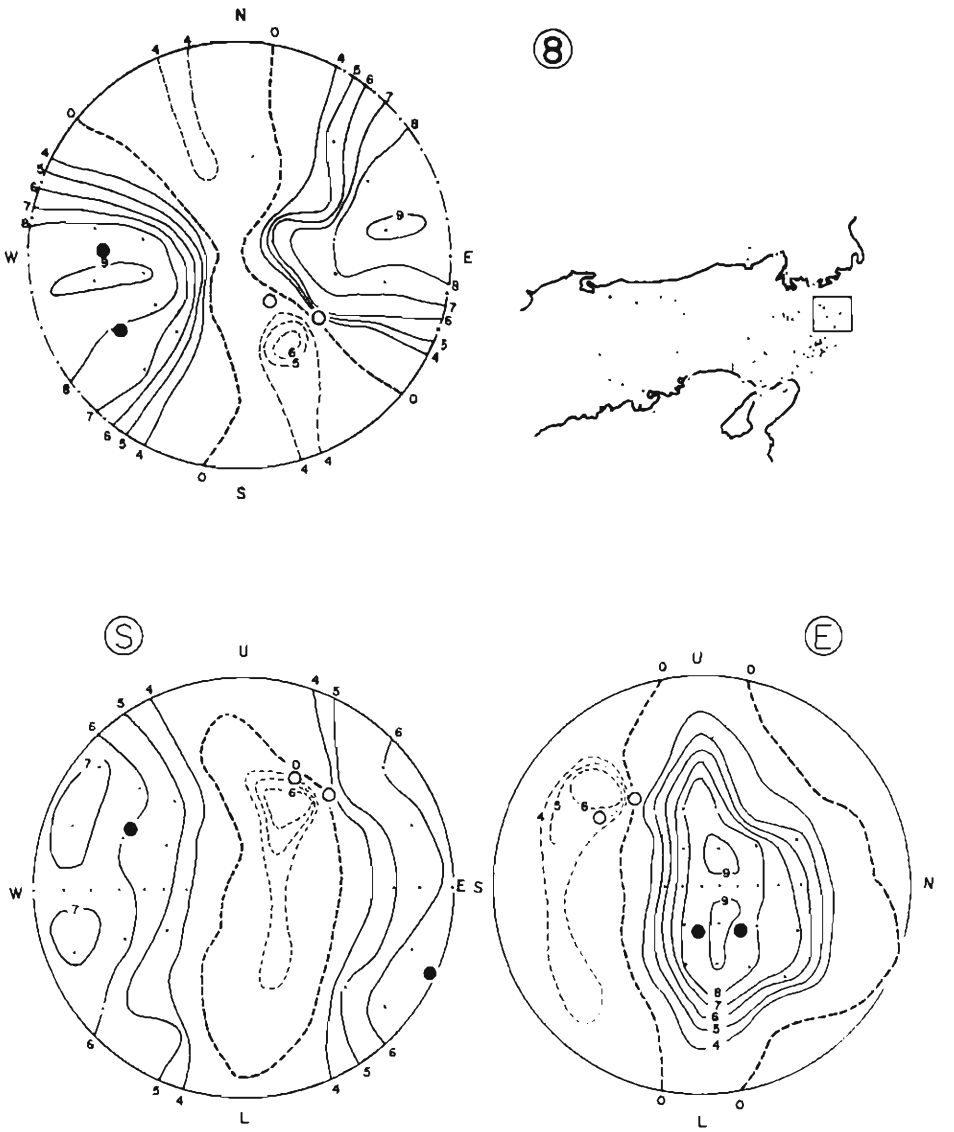

Fig. 15 (a) Smoothed radiation pattern of Region 8. The expression is the same as Fig. 7(a).

compared with the negative zone, it is caused by the fact that many observation stations are located in the dilatation zone on a focal sphere.

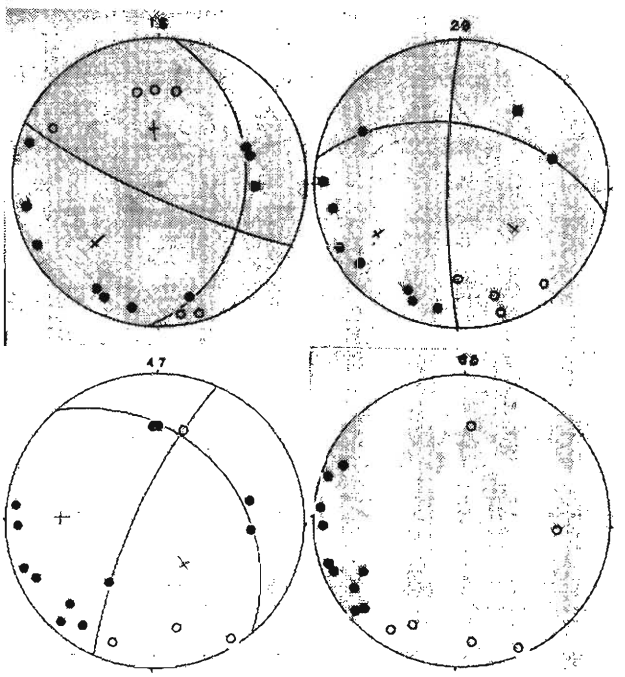

Fig. 15 (b) Individual fault plane solution and distribution of initial P motions projected by Wulff's net. The expression is the same as Fig.7(b). (Region 8)

(j) Region 9, Northern Osaka and Southern Kyoto Pref. (No. 2, 4, 5, 6, 9, 13, 14, 19, 20, 26, 27, 28, 32, 36, 40, 41, 42, 49, 51, 64)

The results obtained are shown in Fig.16(a) and(b). Almost all earthquakes show focal mechanisms of the strike slip fault type, but some earthquakes showed dip angles of about 20° eastward. Only one earthquake, No.51, has the focal mechanism of dip slip fault type with E–W compression. From the analysis of smoothed radiation

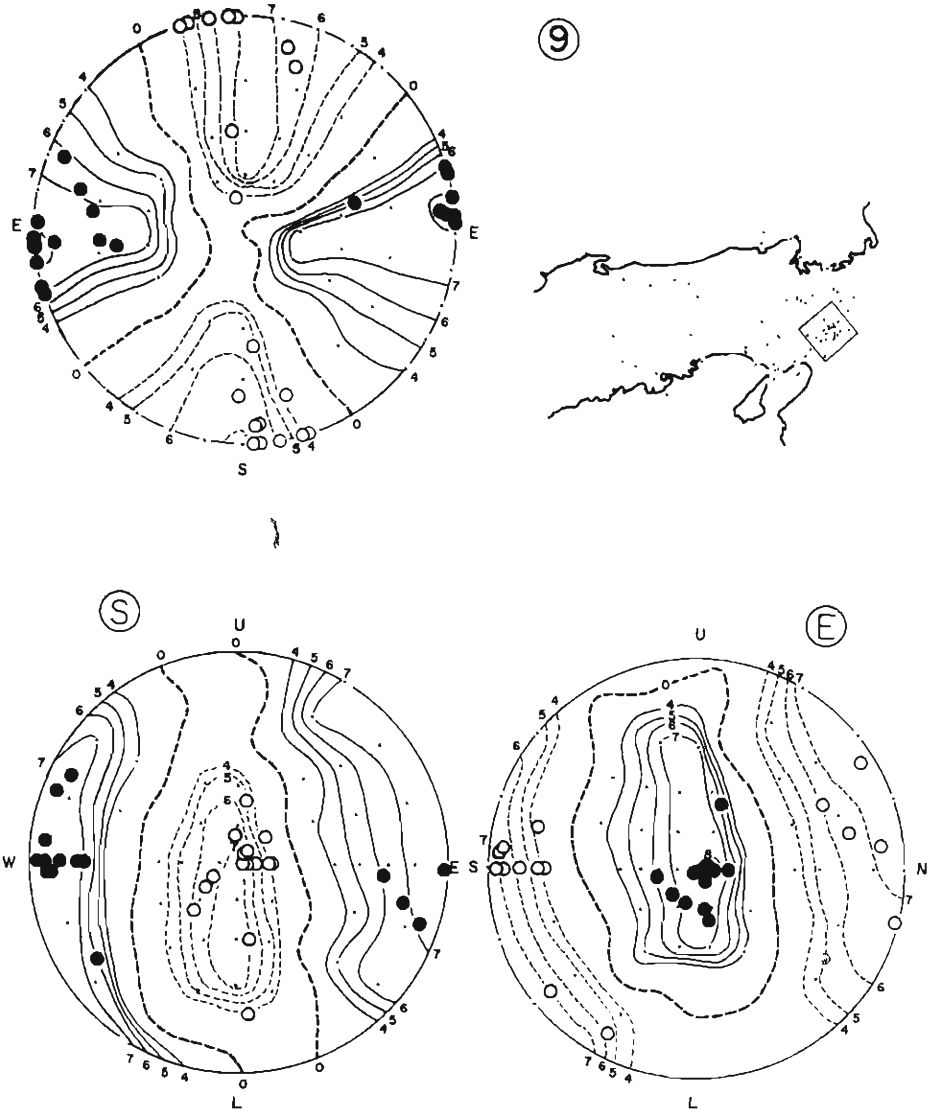

Fig. 16 (a) Smoothed radiation pattern of Region 9. The expression is the same as Fig. 7(a).

pattern, zones of principal stresses show high concentration, of which the maximum value and minimum value are 0.8 and −0.7, respectively. The maximum pressure axis lies nearly horizontally in the E-W direction, and the minimum pressure axis lies nearly horizontally in the N-S direction. But the shape of contours is somewhat slender in comparison with those of the maximum pressure.

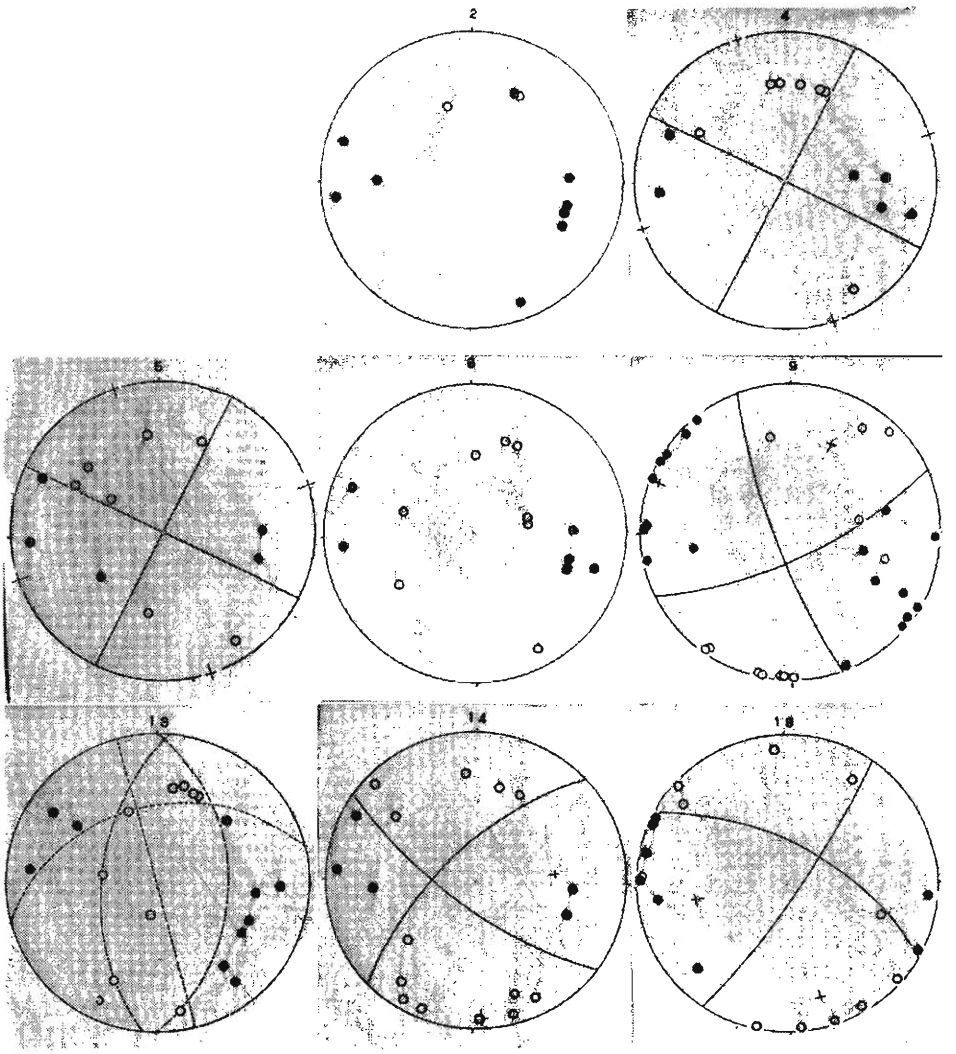

Fig. 16 (b) Individual fault plane solution and distribution of initial P motion projected by Wulff's net. The expression is the same as Fig.7(b). (Region 9)

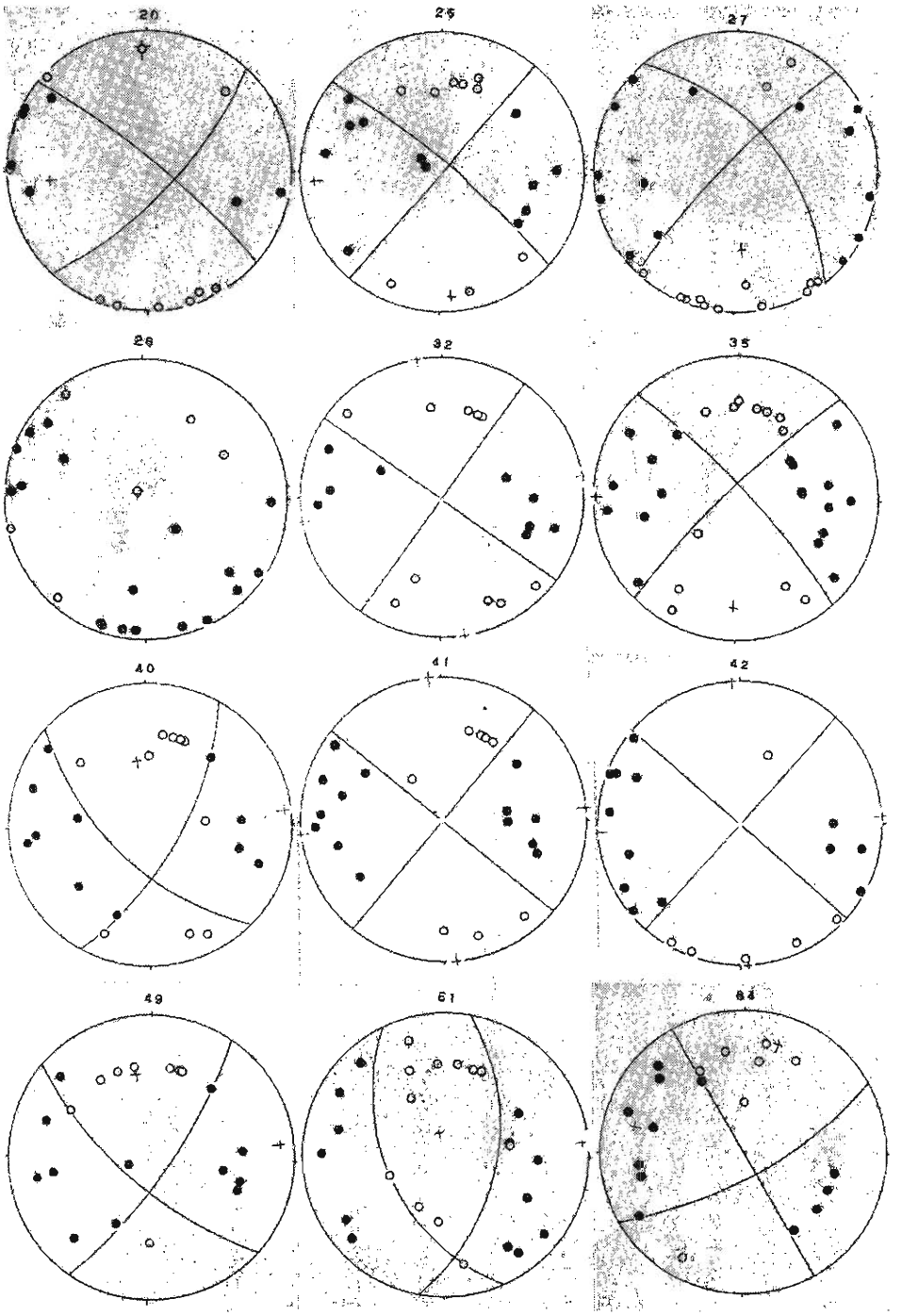
20
25
27
28
32
35
40
41
42
49
61
64

(k) Region 10, (Regions 4 and 5)

We have discussed properties of earthquake generating stresses in various regions using smoothed radiation patterns and fault plane solutions of individual earthquakes. Next, we shall try to superpose some neighbouring regions, in order to know whether stresses acting in a region are equal to stresses in neighbouring regions or not.

The result obtained by superposing Region 4 and 5 is shown in Fig.17. The maximum pressure axis coincides with ones which are decided in respective regions,

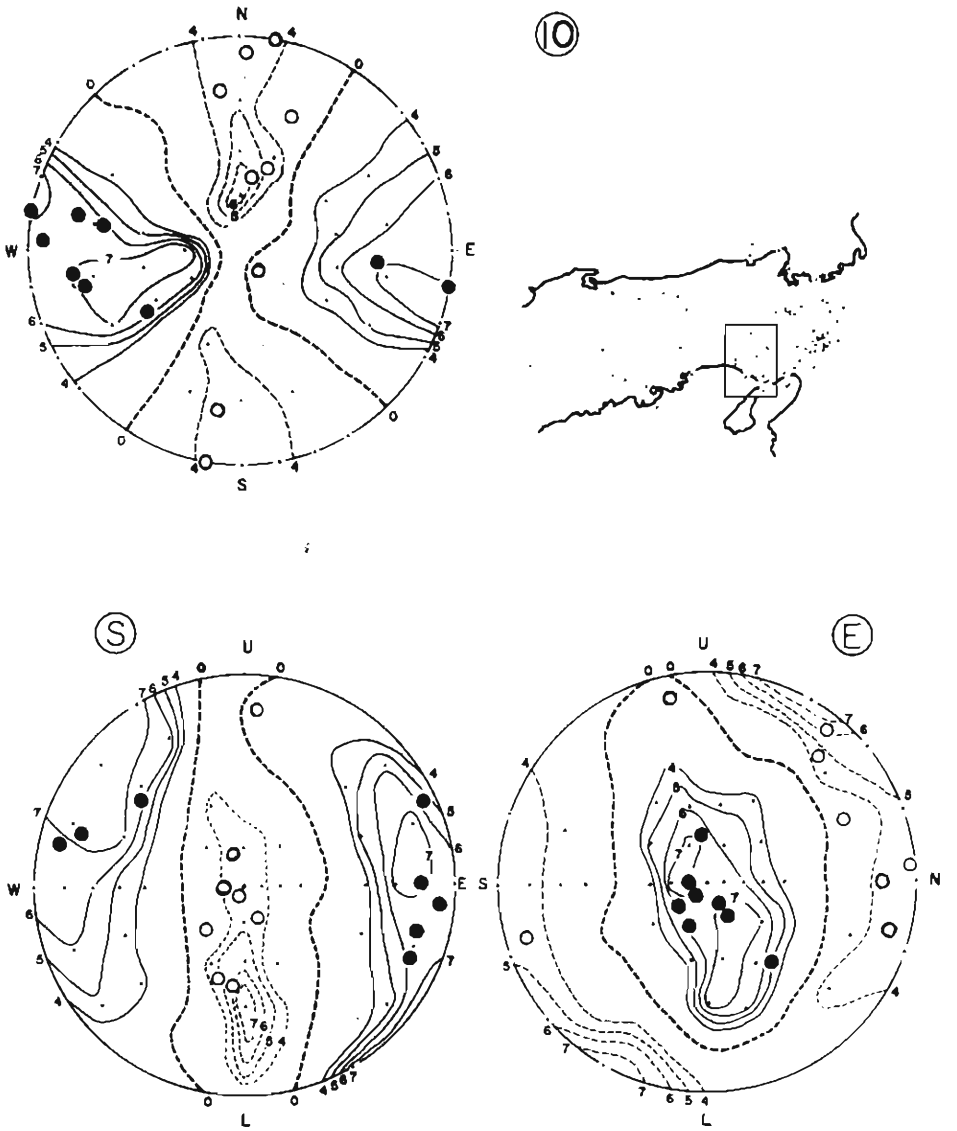

Fig. 17 Smoothed radiation pattern of Region 10. The expression is the same as Fig. 7(a).

being nearly in an E–W direction with a dip angle of 10° eastward. But the minimum pressure axis is concentrated around a location of dip angle of 60° in the N–S direction, and coincides better with Region 4 than with Region 5. Therefore it may be inferred that E–W compression is acting equally in these two regions.

(*l*) *Region 11 (Region 5 and 6)*

Fig. 18 shows a smoothed radiation pattern obtained by superposing Regions 5

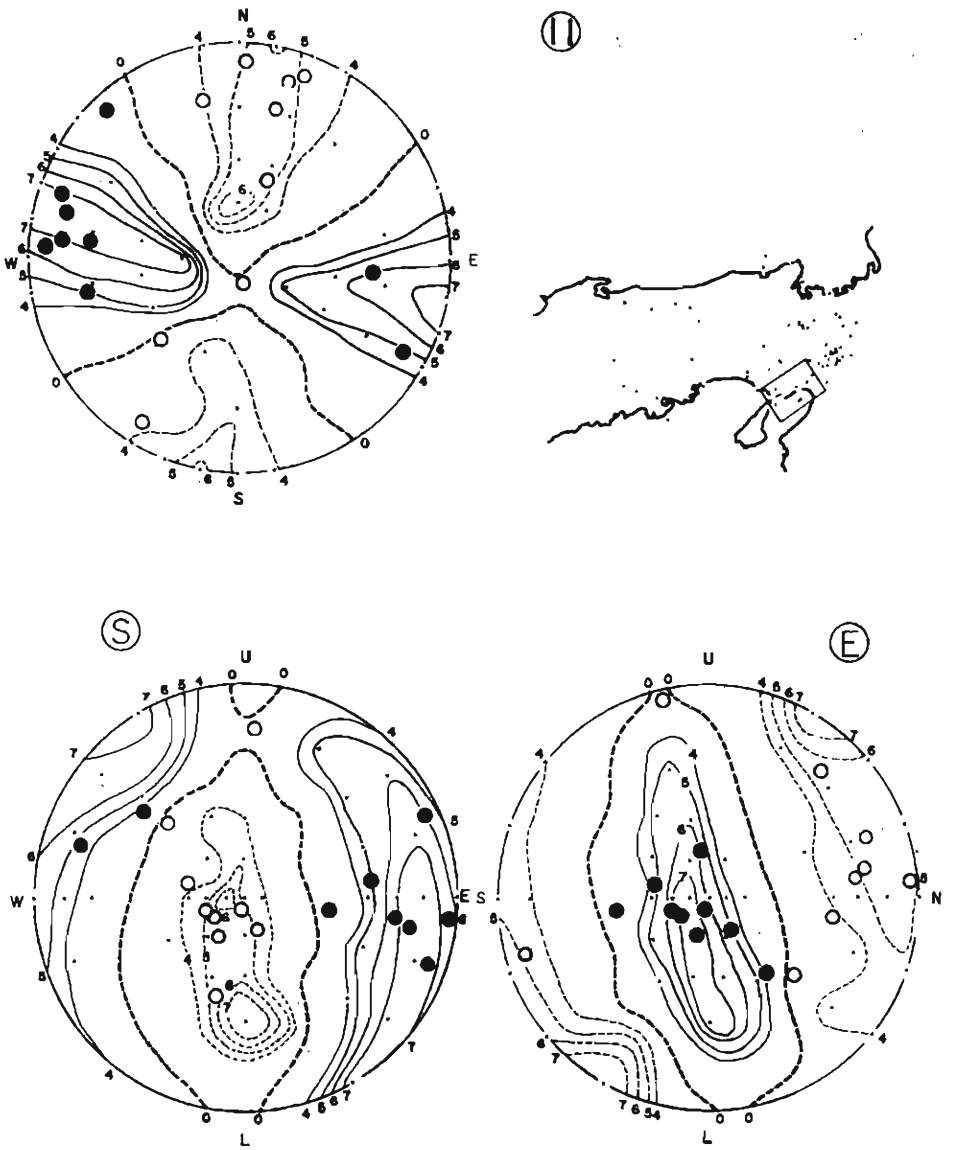

Fig. 18 Smoothed radiation pattern of Region 11. The expression is the same as Fig. 7(a).

and 6. It is recognized that distributions of the maximum pressure zone are rather slender, suggesting that the tectonic stress is not equal in two regions.

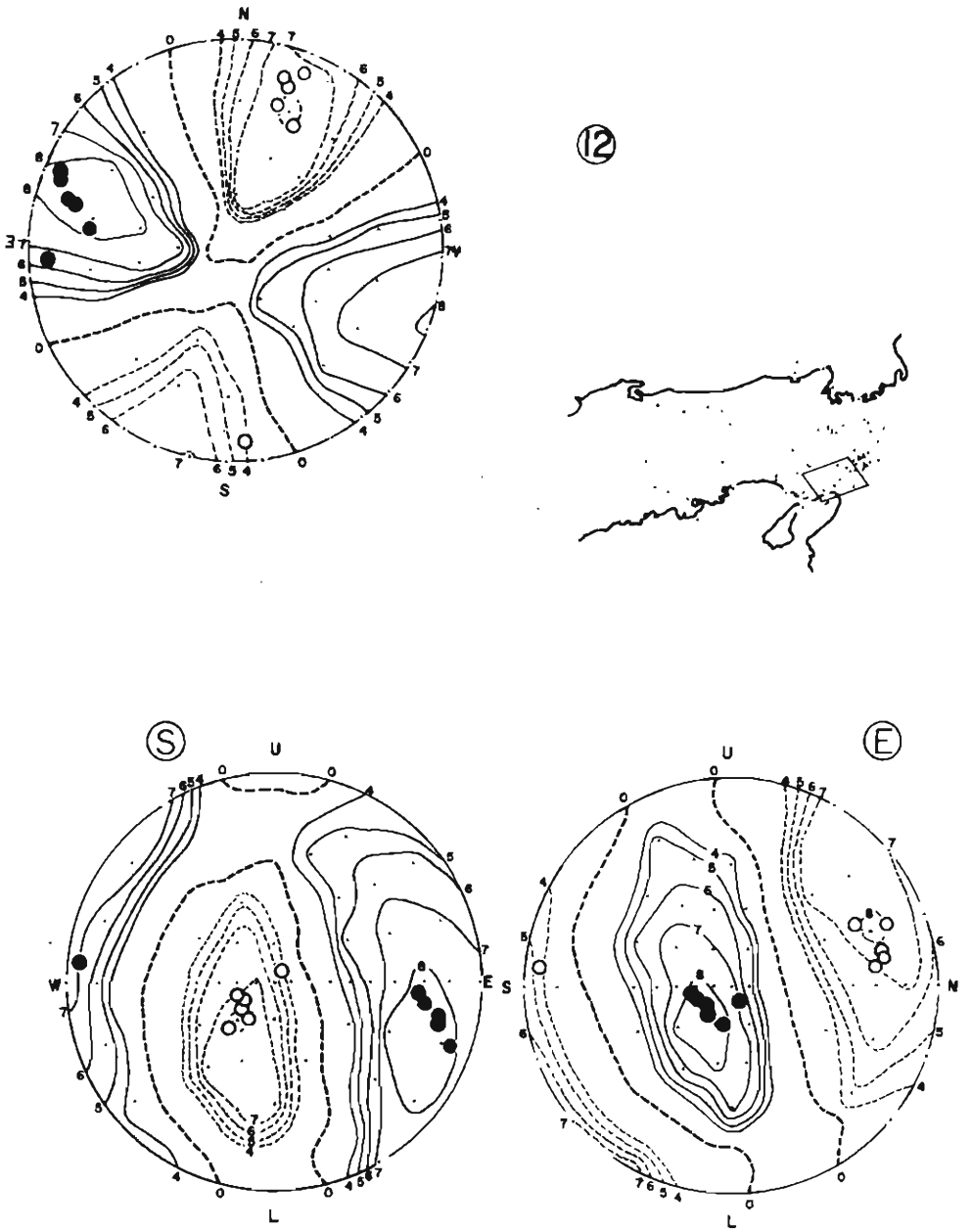

Fig. 19 Smoothed radiation pattern of Region 12. The expression is the same as Fig. 7(a).

(*m*) *Region 12 (Region 6A and 9A)*

Smoothed radiation pattern superposed of two regions is shown in Fig. 19. It shows high concentrations of both the maximum and minimum K-value contours. Focal mechanisms of respective earthquakes are also nearly equal. Since this pattern is equal to the one of Region 6, it is inferred that the same stress as acting in Rokko region is also prevailing in the northern Osaka Pref..

(*n*) *Other Earthquakes* (No. 1, 17, 59)

Fault plane solutions and distributions of initial P motions are shown in Fig. 20. Earthquakes No. 1 and 59 are relatively deep-seated, 27 km and 33 km, compared with other earthquakes. Earthquake, No. 1, has the focal mechanism of a dip slip fault type. For No. 59 all initial P motions showed compression except one observation station. It is impossible to analyze earthquake No. 17, because its epicenter is isolated from analyzed areas and observation data are few.

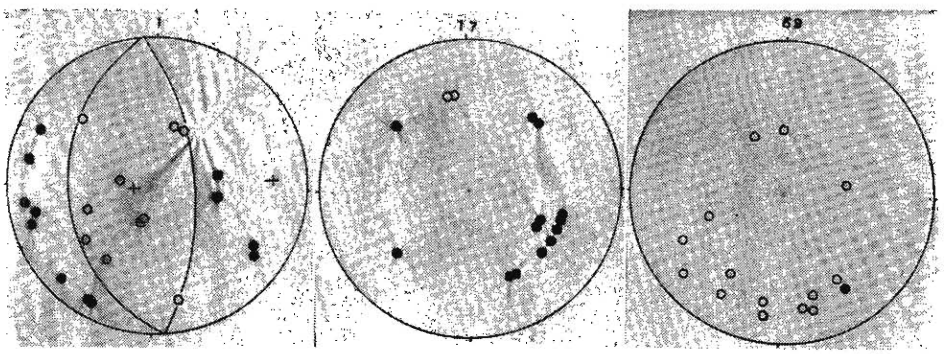

Fig. 20 Fault plane solution and distribution of initial P motion projected by Wulff's net. The expression is the same as Fig. 7(b).

4. General aspect of earthquake generating stress and concluding remarks.

In the preceding section, we mentioned the earthquake generating stress in respective small regions from two viewpoints of fault plane solutions and smoothed radiation patterns. In the following, we shall discuss the stress state prevailing in the whole area concerned.

Fig. 21 shows the smoothed radiation pattern as a whole. It is found that contours

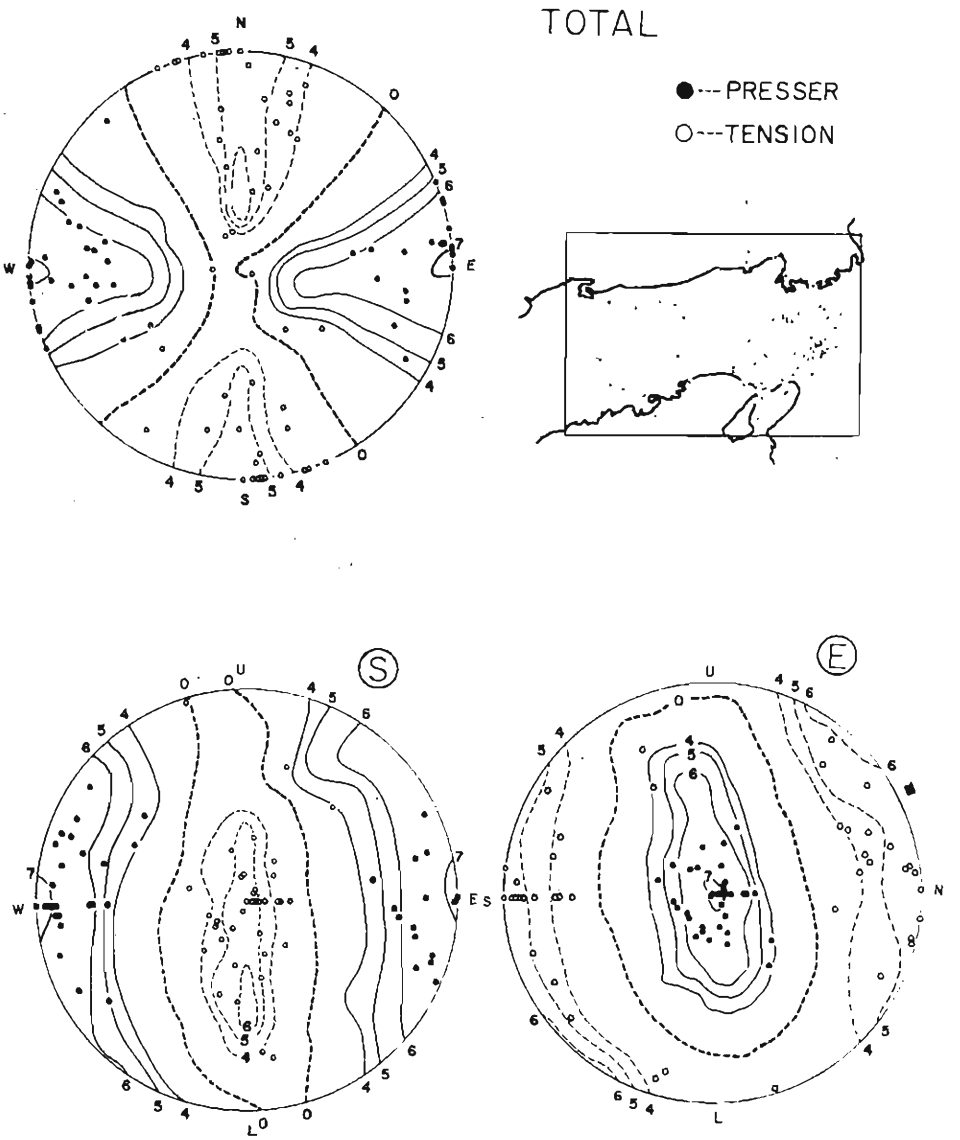

Fig. 21 Smoothed radiation pattern of the whole region. The expression is the same as Fig. 7(a).

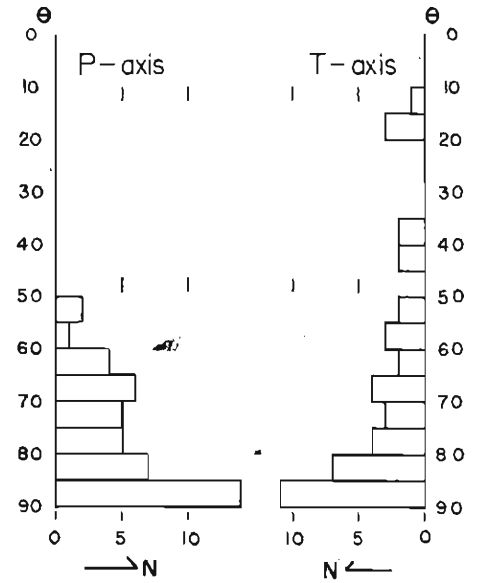

Fig. 22 (a) Distribution of dip angle components of principal stress axes on a fault plane solution. θ is measured downward from the vertical.

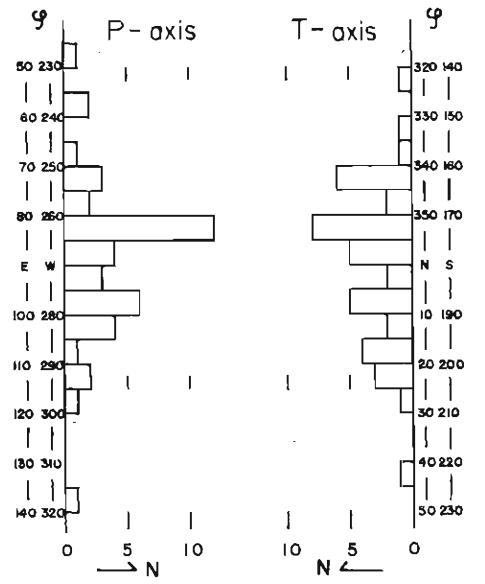

Fig. 22 (b) Distribution of azimuth components of principal stress axes on a fault plane solution. φ is measured clockwise from the north.

of positive K-values are highly concentrated, so that the maximum pressure axis is confidently presumed to lie in the E–W direction horizontally. On the other hand, th shape of contours of negative K-values is somewhat slender in the N–S direction, suggesting that the minimum pressure axis varies in a vertical plane of N–S trend. The distribution of dip angles of the principal axis derived from individual earthquake is shown in Fig. 22(a). As shown in the figure, the dip angle of the maximum pressure axis is displaced from the horizontal ($\theta = 90°$) to $\theta = 50°$, while that of the minimum pressure is greatly displaced from the horizontal to $\theta = 10°$. Fig. 22(b) shows a distribution of azimuths of the principal axes. Two peaks are found, one of which is at about 10° clockwise from E–W and another at about 10° counterclockwise from E–W. These facts suggest that earthquake generating stress acting in the eastern Chugoku and the northern Kinki Districts is horizontal and E–W compression, and the corresponding fault types are strike slip and dip slip.

In Fig. 23, distribution of the smoothed radiation pattern is summarized. It is recognized that stress state differs slightly from region to region, although the mean state is considered to be an E–W compression as noted above. The direction of the maximum pressure axis turns gradually clockwise from northern part to southern ones. Fig. 24 shows a distribution of fault plane solutions in the whole region. Fault plane solutions with nearly vertical null vector are mainly found in Wachi region and

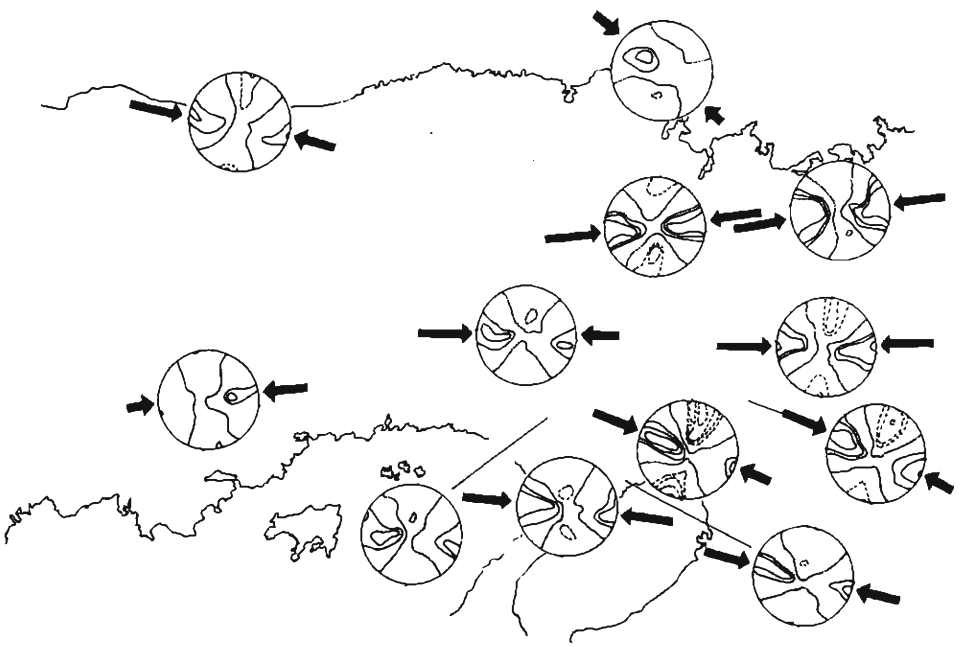

Fig. 23 Distribution of smoothed radiation patterns in whole region. Heavy solid lines with arrow heads indicate the direction of axes of the maximum pressure, and solid and dashed lines indicate equal K-valur lines when the absolute K-value are more than 0.6. The dotted lines indicate lines of K-value = 0.0.

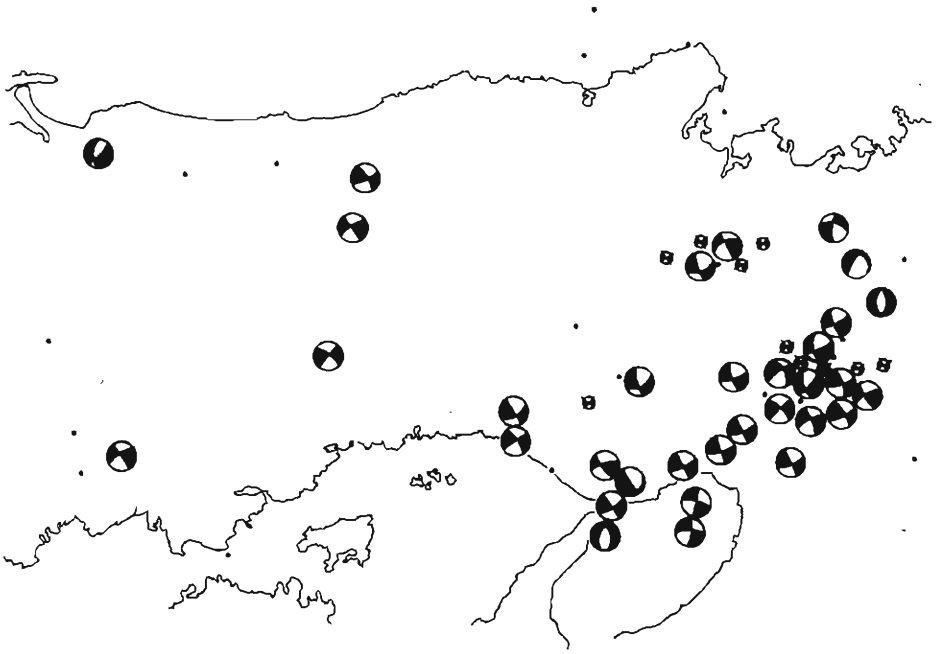

Fig. 24 Distribution of fault plane solutions of respectiue earthquakes in the whole region. Circles indicate fault plane solutions projected by Wullf's net and in respective circles black and white parts indicate dilatation and compression zones.

southern part of Kyoto Pref. along the Yodo-River. Earthquakes of the dip-slip type were detected in western Tottori Pref., Akashi Straits and northern part of Kyoto Pref.. Earthquakes in the Rokko area have a similar focal mechanism to each other and one of the nodal planes lies nearly in ENE–WSW direction which corresponds to the trends of faults in this area. On the contrary, at the junction of two fault systems or earthquake belts such as Akashi Straits, the focal mechanisms seem to have some differences from each other.

These variations of fault plane solutions and smoothed radiation patterns with regions may be related to geological structures of respective regions. For example, referring to Fig. 25, which is the distribution of young fractures elaborated by Huzita[18], we shall be able to recoginize some relations between earthquake mechanism and geological structure. These relations, of course, must be treated in more detail and will be discussed in our succeeding paper. However, we may conclude here that earthquake generating stress in the area concerned is E–W compression, and that geological structures play an important role in determining earthquake mcehanism.

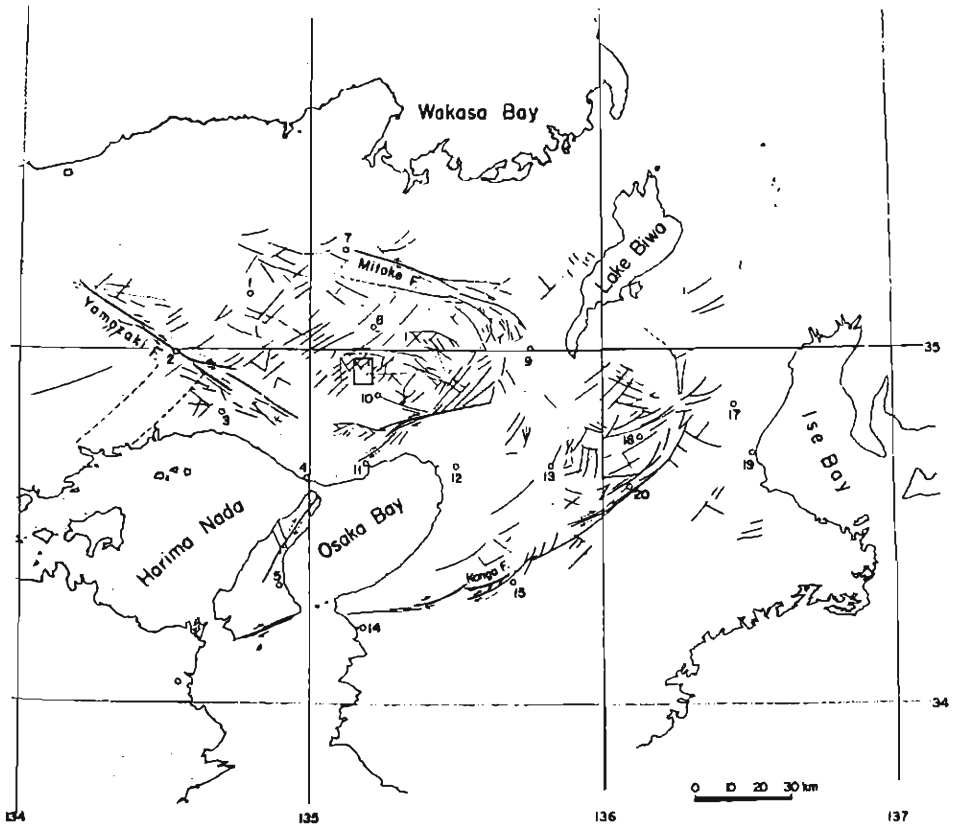

Fig. 25 Map of the distribution of the youngest fractures in the district. (after Huzita, 1969)

Acknowledgement

The author wishes to express his thanks to Prof. Y. Kishimoto for his suggestions and encouragement throughout this study. The author is also indebted to Dr. J. Miyakoshi, Dr. T. Mikumo, Dr. K. Oike and Mr. M. Nakamura for their valuable discussions, and to Mr S. Nakao, Mr. S. Yabe and Miss Y. Tsushima for their assistances in the analysis. The Wakayama, Shiraki, Kochi and Abuyama Observatories kindly allowed the use of thier observational data. Computations were made by a FACOM-230-60 at the Computation Center, Kyoto University.

References

1) Hashizume, M. : Investigation of Microearthquakes - On Seismicity -, Bull. Disas. Prev. Res. Inst., Kyoto Univ., Vol. 19, 1969, pp.63-81.
2) Hashizume, M. : Investigation of Microearthquakes - On the Nature of the Crust -, Bull. Disas. Prev. Res. Inst., Kyoto Univ., Vol. 20, 1970, pp.53-64.
3) Hashizume, M. : Investigation of Microearthquakes - On Earthquake Occurrence in the

Crust –, Bull. Prev. Res. Inst., Kyoto Univ., Vol. 20, 1970, pp.65-94.
4) Ichikawa, M. : Statistical Investigation of Mechanism of Earthquakes Occurring in and near Japan and Some Related Problems, Pap. Met. Geophys., Vol. 18, 1966, pp.1-72 (in Japanese).
5) Aki, K. : Earthquake Generating Stress in Japan for the Years 1961 to 1963 Obtained by Smoothing the First Motion Radiation Patterns, Bull. Earthq. Res. Inst., Vol. 44, 1966, pp. 447-471.
6) Nakamura, M. : On the Focal Mechanism in Central Kinki District, Wakayama Rep., Vol. 2, 1971,
7) Huzita K. : Tectonic Development of Southwest Japan in the Quatornary Period, Jour. Geosience, Osaka City Univ., Vol. 12, 1969, pp.53-70.
8) Shiono, K. : Focal Mechanism of Local Earthquakes in Wakayama Region (Part. 1), Jour. Seismol. Soc. Jap., Vol. 23, 1970, pp.226-236 (in Japanese).
9) Shiono, K. : Focal Mechanism of Local Earthquakes in Wakayama Region (Part. 2), Jour. Seismol. Soc. Jap., Vol. 23, 1970, pp.253-263 (in Japanese).
10) Shiono, K. : Focal Mechanism of Small Earthquakes in the Kii Peninsula, Kii Channel and Shikoku, Southwest Japan, and Some Problems related to the Plate Tectonics, Jour. Geosience, Osaka City Univ., Vol. 16, 1973.
11) loc. cit. 1).
12) Tsumura, K. : Determination of Earthquake Magnitude from Total Duration of Oscillation, Bull. Earthq. Res. Inst., Vol. 45, 1967, pp.7-18.
13) loc. cit. 1).
14) loc. cit. 5).
15) Oike, K. : Distribution of Earthquake Generating Stresses Obtained by Smoothing the First Motion Pattern, Jour. Phy. Ear., Vol. 19, 1971, pp.181-198.
16) loc. cit. 5).
17) Nishida, R. : Activity of Earthquakes occurred in April 1970 near Funaoka Station, Disas. Prev. Res. Inst. Annuals, No. 14, 1970, pp.1-11 (in Japanese).
18) loc. cit. 7).